Magnetic excitations in L-edge resonant inelastic x-ray scattering from cuprate compounds

Jun-ichi Igarashi Faculty of Science, Ibaraki University, Mito, Ibaraki 310-8512, Japan

Tatsuya Nagao
Faculty of Engineering, Gunma University, Kiryu, Gunma 376-8515, Japan
(Dated: September 19, 2018)

We study the magnetic excitation spectra in L-edge resonant inelastic x-ray scattering (RIXS) from undoped cuprates. We analyze the second-order dipole allowed process that the strong perturbation works through the intermediate state in which the spin degree of freedom is lost at the core-hole site. Within the approximation neglecting the perturbation on the neighboring sites, we derive the spin-flip final state in the scattering channel with changing the polarization, which leads to the RIXS spectra expressed as the dynamical structure factor of the transverse spin components. We assume a spherical form of the spin-conserving final state in the channel without changing the polarization, which leads to the RIXS spectra expressed as the 'exchange'-type multi-spin correlation function. Evaluating numerically the transition amplitudes to these final states on a finite-size cluster, we obtain a sizable amount of the transition amplitude to the spin-conserving final state in comparison with that to the spin-flip final state. We treat the itinerant magnetic excitations in the final state by means of the 1/S-expansion method. Evaluating the higher-order correction with 1/S, we find that the peak arising from the one-magnon excitation is reduced with its weight, and the continuous spectra arising from the three-magnon excitations come out. The interaction between two magnons is treated by summing up the ladder diagrams. On the basis of these results, we analyze the L_3 -edge RIXS spectra in $Sr_2CuO_2Cl_2$ in comparison with the experiment. It is shown that the three-magnon excitations as well as the two-magnon excitations give rise to the intensity in the high energy side of the one-magnon peak, making the spectral shape asymmetric with wide width, in good agreement with the experiment.

PACS numbers: 78.70.Ck, 72.10.Di, 78.20.Bh, 74.72.Cj

I. INTRODUCTION

Resonant inelastic x-ray scattering (RIXS) has recently attracted much interest as a useful tool to investigate excited states in solids. The K- and L-edge resonances have been widely used in transition-metal compounds. When one tries to interpret the experimental results, some theoretical support becomes inevitable. Since the intermediate states involved in the scattering process at the K- and L-edges are different from each other, the theoretical analysis should discriminate the difference with great care.

The K-edge resonance is more suitable than the L-edge to detect the momentum dependence of the spectra, since the wavelength of the K-edge x-ray is an order of the lattice constant. In the K-edge RIXS, the 1s-core electron is prompted to an empty 4p state by absorbing photon, then charge excitations are created in order to screen the core-hole potential, and finally the photo-excited 4p electron is recombined with the core hole by emitting photon. Charge excitations are finally left with energy and momentum transferred from photons. $^{1-7}$ The spectra have been analyzed by several methods. $^{8-11}$ Among them, a formalism developed by Nomura and Igarashi (NI) $^{12-14}$ usefully describes the RIXS spectra in terms of the 3d-density-density correlation function on the initial state. 15 It is based on the Keldysh Green function, 16 and is re-

garded as an adaption of the resonant Raman theory of Nozières and Abrahams. 17 In the actual application of the formalism, the electronic states are described within the Hartree-Fock approximation on the multiband tight-binding model, and the electron correlation is treated within the random phase approximation. The spectra are calculated as functions of energy loss and momentum transfer in good agreement with the experiments for undoped cuprates, $^{12-14}$ NiO, 18 and LaMnO₃. 19

In addition to the charge excitations, the magnetic excitations have been observed from the Cu K-edge RIXS experiment in La₂CuO₄.^{20,21} They are brought about through the modification of the exchange coupling between the spins of 3d electrons at the corehole site and those at the neighboring sites by the core-hole potential.^{22–24} To investigate the magnetic excitation spectrum, the NI formula has been adapted in our previous work.²⁵ By replacing the channel of creating an electron-hole pair by that of creating two magnons, the expression is derived that the RIXS spectra are proportional to the two-magnon correlation function. The magnon-magnon interaction in the correlation function has been treated with the use of the 1/Sexpansion method (S is the magnitude of spin). $^{26-31}$ The obtained spectra, reflecting a significant influence from the magnon-magnon interaction, show characteristic dependence on the energy loss and the momentum transfer, which captures features the experimental data have

demonstrated.^{20,21}

Unlike the K-edge RIXS, the L-edge RIXS directly accesses the 3d states, which leads us to a necessity to develop an appropriate treatment for the L-edge RIXS. The process is illustrated for undoped cuprates in Fig. 1; the 2p-core electron is prompted to the empty $x^2 - y^2$ orbital by absorbing photon, and then an occupied 3d electron combines with the core hole by emitting photon. Here x, y, and z axes correspond to the crystal axes a, b, and c, respectively. If the 3d state in the photo-emitting process is different from the $x^2 - y^2$ orbital [Fig. 1 (a)], excitations within the 3d states are left in the final state, which process is called the 'd-d' transition.³² Since such excited states are quite localized at the core-hole site, the spectra show little momentum dependence. In this paper, skipping the study of the d-d transition, we concentrate on the study of the L-edge RIXS spectra arising from magnetic excitations, which have recently been observed in undoped cuprates. 33–35

It is known that the spin-flip excitations [Fig. 1(b)] give rise to the spin-wave-like dispersion, when the direction of the staggered moment deviates from the z direction.³⁶ Since the spin angular-momentum is coupled to the orbital angular-momentum through the large spin-orbit interaction of the 2p-core states, the change by the spin-flip may be compensated by the change of the polarization of photon. In addition, it is expected that the spin-conserving excitations [Fig. 1(c)] could be brought about through the intermediate state, since the strong perturbation is working by losing the spin degree of freedom at the core-hole site in the intermediate state.

For investigating the magnetic excitations, the RIXS spectra have been analyzed by assuming an extreme condition that the core-hole life-time is so short that the intermediate state can not have enough time to relax.¹¹ Only the one-magnon excitation is brought about without any two-magnon excitations. This is called as the ultra-short core-hole life-time (UCL) approximation,³⁶ which reminds us of the fast collision approximation in resonant elastic x-ray scattering.^{37,38} In reality, the spectra observed as a function of energy loss exhibit a systematic change with changing momentum transfer;³⁵ the peak position moves according to the spin-wave dispersion curve, while their shapes exhibit structures indicative of two- or three-magnon excitations. Accordingly the assumed condition is obviously unsatisfied in undoped cuprates. The purpose of this paper is to develop a comprehensive theory describing the spectra beyond the UCL approximation.

The situation that the spin degree of freedom is lost at the core-hole site in the intermediate state is similar to the situation of the non-magnetic impurity, which problem has been extensively studied by the linear-spin-wave (LSW) method.^{39,40} The method developed there, however, is not applicable to the present problem, since the calculation of the RIXS spectra require not alone the intermediate state but also the initial and final states in evaluating overlaps between them. It may not be logi-

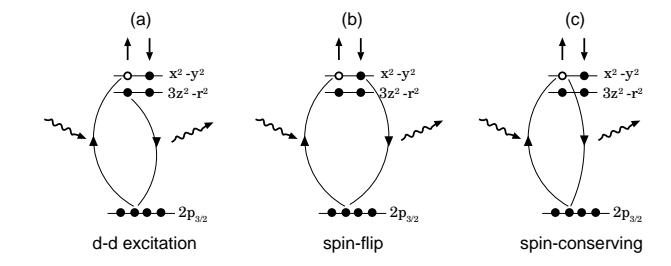


FIG. 1: L_3 -edge RIXS process for undoped cuprates. Black and white circles represent electrons and holes, respectively. Vertical arrows indicate the spin direction. Wavy lines indicate the incident and scattered photon. The t_{2g} orbitals are omitted.

cally appropriate to perform a perturbation calculation with the terms involving the lost spin degree of freedom, although such attempts have been mentioned and tried.⁴¹ Along this consideration, the perturbative expansion like the NI formula may not be sufficient to treat the intermediate state.

In this paper, we analyze the second-order dipole allowed process that the strong perturbation works through the intermediate state. Within the approximation that the perturbation is not extending to neighboring sites, we derive the spin-flip final state expressed as $\alpha_{f\perp}$ × $\alpha_{i\perp}\cdot \mathbf{S}_0|g\rangle$ in the scattering channel with changing the polarization, where $\alpha_{i(f)\perp}$ is the polarization vector of incident (scattered) photon projected onto the x-y plane, and S_0 is the spin operator vector at the core-hole site. This form is inferred from the formula of the elastic scattering. 42,43 This final state leads to the RIXS spectra expressed as the dynamical structure factor of the transverse spin component. In the scattering channel with changing the polarization, we assume a spherical form of the spin-conserving final state, which leads to the RIXS spectra expressed as the 'exchange'-type multi-spin correlation function. In the evaluation of the transition amplitude to these final states, we introduce a finite-size cluster and use the wave-functions numerically obtained by diagonalizing the Hamiltonian. We obtain a sizable amount of the transition amplitude to the spin-conserving final state in comparison with that to the spin-flip final state.

We express the spin-flip and spin-conserving final states in terms of magnon creations and annihilations with the systematic use of the 1/S expansion. The spin-flip operators S^{\pm} are expanded in terms of one-magnon creation and annihilation operators within the LSW theory, and of three-magnon creation and annihilation operators in the second order of 1/S. $^{28-30,44,45}$ Hence the spin-flip final state gives rise to the RIXS spectra consist of two ingredients. One is the δ -function peak with its weight reduced from the LSW value and the other is the broad three-magnon continuum as a function of energy loss. The spin-conserving operators are expanded in terms of two-magnon creation and annihilation operators with neglecting the higher-order terms such as four-magnon creation and annihilation operators. Since

two magnons are created near the core-hole site, we take account of their interaction by summing up the ladder diagrams, as was done in the magnetic excitation spectra in the K-edge RIXS.²⁵

On the basis of these results, we analyze the Cu L_3 -edge spectra of $\mathrm{Sr_2CuCl_2O_2}$, which show strong dependence on the polarization in accordance with the experiment.³⁵ We find that a considerable amount of satellite intensity comes from the three-magnon excitations in the spin-flip final state, which leads to the asymmetric shape as a function of energy loss in the π polarization. We also obtain the substantial contribution from the two-magnon excitations in the σ polarization. These results agree well with the experiment.

The present paper is organized as follows. In Sec. II, we describe the Hamiltonian responsible for magnetic excitations and transition-matrix elements relevant to the $L_{2,3}$ edges in cuprate compounds. In Sec. III, we discuss the process giving rise to the magnetic excitations through the intermediate state. The RIXS spectra are expressed in terms of spin-correlation functions. In Sec. IV, spin-correlation functions are calculated by means of the 1/S expansion. In Sec. V, the calculated L_3 -edge spectra of Cu are compared with those for $Sr_2CuO_2Cl_2$. Section VI is devoted to the concluding remarks. In Appendix, a brief summary of the 1/S-expansion method is given.

II. FORMULATION OF RIXS SPECTRA AT THE $L_{2,3}$ EDGE

A. Hamiltonian

At the half-filling in cuprate compounds, each Cu atom has one hole in the x^2-y^2 orbital, where the x and y axes are defined along the Cu-O bonds and the z along the crystal c axis. Adopting the hole picture, we assume a single band Hubbard model on a two-dimensional square lattice for 3d electrons:

$$H = t \sum_{\langle i,j \rangle, \sigma} (d_{i\sigma}^{\dagger} d_{j\sigma} + \text{H.c.}) + U \sum_{i} d_{i\uparrow}^{\dagger} d_{i\downarrow}^{\dagger} d_{i\downarrow} d_{i\uparrow}, \quad (2.1)$$

where $d_{i\sigma}$ ($d_{i\sigma}^{\dagger}$) represents the annihilation (creation) operator of the hole with spin σ at site i. The sum over $\langle i,j\rangle$ extends over distinct pairs of nearest neighbors. Hopping integral and on-site Coulomb interaction are denoted as t and U, respectively. We have neglected the small interlayer coupling. This Hubbard model may be mapped from a more precise "d-p" model for cuprate compounds.

For low-energy spin excitations, the Hubbard Hamiltonian is further mapped onto the two-dimensional Heisenberg Hamiltonian with the exchange coupling constant $J=4t^2/U$,

$$H_{\text{mag}} = J \sum_{\langle i,j \rangle} \mathbf{S}_i \cdot \mathbf{S}_j. \tag{2.2}$$

This Hamiltonian leads to an antiferromagnetic order. It is known that Cu spins align on the CuO₂ plane at the angle of $\pi/4$ to the Cu-O bonds. 46 Therefore, it is convenient to define the spin coordinate frame x', y', z' axes by rotating the crystal-fixed coordinate frame a, b, c axes through the Euler angles $\alpha = \pi/4$, $\beta = \pi/2$, and $\gamma = 0$. The \uparrow and \downarrow states in Eq. (2.1) are interpreted as the eigenstates with respect to $S^{z'}$. Hereafter, we shall describe the spin state of the 3d electron in the x'y'z' coordinate.

B. E1 transition at the $L_{2,3}$ edge

The Hamiltonian of photon may be written as

$$H_{\rm ph} = \sum_{\mathbf{q},\mu} \omega_{\mathbf{q}} c_{\mathbf{q}\mu}^{\dagger} c_{\mathbf{q}\mu}, \qquad (2.3)$$

where $c_{\mathbf{q}\mu}$ ($c_{\mathbf{q}\mu}^{\dagger}$) stands for the annihilation (creation) operator of the photon with momentum q, energy $\omega_{\mathbf{q}}$, and polarization direction μ (= x, y, and z). In the electric dipole (E1) transition, a 2p-core electron is excited to the 3d states at the transition-metal $L_{2,3}$ edge. The 2pstates are characterized by the total angular momentum j = 3/2 and 1/2 due to the strong spin-orbit interaction. The eigenstates with j = 3/2 may be expressed as $|\phi_1 \uparrow\rangle$, $\sqrt{1/3}|\phi_1\downarrow\rangle + \sqrt{2/3}|\phi_0\uparrow\rangle$, $\sqrt{2/3}|\phi_0\downarrow\rangle + \sqrt{1/3}|\phi_{-1}\uparrow\rangle$, $|\phi_{-1}\downarrow\rangle$, for m=3/2,1/2,-1/2,-3/2, respectively, and those with j=1/2 may be expressed as $-\sqrt{2/3}|\phi_1\downarrow$ $\rangle + \sqrt{1/3} |\phi_0 \uparrow\rangle, -\sqrt{1/3} |\phi_0 \downarrow\rangle + \sqrt{2/3} |\phi_{-1} \uparrow\rangle, \text{ for } m = 1/2$ and -1/2, respectively, where m represents the magnetic quantum number. The orbitals $\phi_1, \, \phi_0, \, \text{and} \, \phi_{-1}$ have angular dependence Y_{11} , Y_{10} and Y_{1-1} , respectively. In the above expression, the coordinate frame for spin is defined the same as the orbitals, which is different from that for the spins of the 3d states, that is, \uparrow and \downarrow are associated with the direction of the crystal c axis. Therefore, the interaction between photon and electron at site i may be described as

$$H_{\rm int} = w \sum_{\mathbf{q},\mu} \frac{1}{\sqrt{2\omega_{\mathbf{q}}}} \sum_{i,m,\sigma} D^{\mu}(jm,\sigma) h_{jm}^{\dagger} c_{\mathbf{q}\mu} d_{i\sigma} e^{i\mathbf{q}\cdot\mathbf{r}_{i}} + \text{H.c.},$$
(2.4)

where h_{jm}^{\dagger} stands for the creation operator of the 2p hole with the angular momentum jm. The w is a constant proportional to $\int_0^{\infty} r^3 R_{3d}(r) R_{2p}(r) dr$, with $R_{3d}(r)$ and $R_{2p}(r)$ being the radial wave-functions for the 3d and 2p states of Cu atom. The $D^{\mu}(jm,\sigma)$ describes the dependence on the core-hole state and 3d spin, which is calculated by taking care of the difference in the definition of the spin axes between the 3d and 2p states. Table I shows the calculated values of $D^{\mu}(jm,\sigma)$. Note that no E1 transition takes place for the polarization parallel to the z axis.

TABLE I: Numerical values of $D^{\mu}(jm,\sigma)$. Here, $u=\mathrm{e}^{i(\alpha+\gamma)/2}\cos\frac{\beta}{2}$ and $v=\mathrm{e}^{i(\gamma-\alpha)/2}\sin\frac{\beta}{2}$, where $\alpha,\ \beta,\ \mathrm{and}\ \gamma$ are the Euler angles transforming the crystal-fixed $a,\ b,\ \mathrm{and}\ c$ axes to the spin axes $x',\ y',\ \mathrm{and}\ z'$ axes.

μ	J	m	$\sigma = \uparrow$	$\sigma = \downarrow$
\boldsymbol{x}	3/2	3/2	$-\frac{1}{\sqrt{10}}u^*$	$\frac{1}{\sqrt{10}}v$
		1/2	$-\frac{1}{\sqrt{30}}v^*$	$-\frac{1}{\sqrt{30}}u$
		-1/2	$\frac{\sqrt{100}}{\sqrt{300}}u^*$	$-\frac{\sqrt{10}}{\sqrt{30}}v$
		-3/2	$\frac{1}{\sqrt{10}}v^*$	$\frac{1}{\sqrt{10}}u$
	1/2	-1/2 -3/2 -1/2	$\frac{\sqrt{15}}{\sqrt{15}}v^*$	$\frac{\sqrt{15}}{\sqrt{15}}u$
		-1/2	$-\frac{1}{\sqrt{10}}u^*$ $-\frac{1}{\sqrt{30}}v^*$ $\frac{1}{\sqrt{30}}u^*$ $\frac{1}{\sqrt{10}}v^*$ $\frac{1}{\sqrt{15}}u^*$ $\frac{1}{\sqrt{15}}u^*$ $\frac{1}{\sqrt{10}}u^*$ $\frac{1}{\sqrt{30}}u^*$ $\frac{1}{\sqrt{30}}u^*$ $\frac{1}{\sqrt{30}}v^*$ $\frac{1}{\sqrt{10}}v^*$ $\frac{1}{\sqrt{15}}v^*$ $\frac{1}{\sqrt{15}}v^*$ $\frac{1}{\sqrt{15}}v^*$	$\begin{array}{c} \frac{1}{\sqrt{10}}v \\ -\frac{\sqrt{30}}{\sqrt{30}}u \\ -\frac{\sqrt{30}}{\sqrt{30}}v \\ \frac{1}{\sqrt{10}}u \\ -\frac{\sqrt{15}}{\sqrt{15}}v \\ -\frac{i}{\sqrt{10}}v \\ -\frac{i}{\sqrt{30}}v \\ -\frac{i}{\sqrt{30}}v \\ -\frac{i}{\sqrt{30}}v \\ -\frac{i}{\sqrt{10}}u \\ -\frac{i}{\sqrt{15}}u \\ -\frac{i}{\sqrt{15}}v \\ -\frac{i}{\sqrt{15}}v \end{array}$
y	3/2	3/2	$\frac{i}{\sqrt{10}}u^*$	$-\frac{i}{\sqrt{10}}v$
		1/2	$\frac{i}{\sqrt{30}}v^*$	$\frac{i}{\sqrt{30}}u$
		-1/2	$\frac{v_i}{\sqrt{30}}u^*$	$-\frac{v}{\sqrt{30}}v$
		-3/2	$\frac{v_{i0}}{\sqrt{10}}v^*$	$\frac{v_{i0}}{\sqrt{10}}u$
	1/2	-1/2 -3/2 -1/2	$-\frac{v_{10}^{10}}{\sqrt{15}}v^{*}$	$-\frac{\sqrt{i}}{\sqrt{15}}u$
		-1/2	$\frac{v_i^{To}}{\sqrt{15}}u^*$	$-\frac{v_{i}}{\sqrt{15}}v$
			0	

C. Formulation of RIXS spectra

Following Noziéres and Abrahams, ¹⁷ we use the Keldysh-Schwinger formalism ¹⁶ to investigate the RIXS spectra. First we prepare the initial state

$$|\Phi_i\rangle = c_{\mathbf{q}_i\alpha_i}^{\dagger}|g\rangle,$$
 (2.5)

where $|g\rangle$ represent the ground state of the matter with energy E_g . The incident photon has momentum \mathbf{q}_i , energy ω_i , and polarization direction α_i . Then we calculate the probability of finding a photon with momentum \mathbf{q}_f , energy ω_f , and polarization direction α_f at time t_0 using the following formula,

$$P_{\mathbf{q}_f \alpha_f; \mathbf{q}_i \alpha_i}(t_0) = \langle \Phi_i | U(-\infty, t_0) c_{\mathbf{q}_f \alpha_f}^{\dagger} c_{\mathbf{q}_f \alpha_f} U(t_0, -\infty) | \Phi_i \rangle.$$
(2.6)

Here U(t,t') is the S matrix defined by

$$U(t, -\infty) = T \exp\left\{-i \int_{-\infty}^{t} H_{\text{int}}(t') dt'\right\}, \qquad (2.7)$$

where $H_{\rm int}(t) = \exp[i(H+H_{\rm ph})t]H_{\rm int}\exp[-i(H+H_{\rm ph})t]$ with H and $H_{\rm ph}$ being the Hamiltonian of matter and photon, and T represents the time-ordering operator.

The S-matrix is expanded up to the second order with H_{int} :

$$U(t, -\infty) = 1 + (-i) \int_{-\infty}^{t} H_{\text{int}}(t') dt' + (-i)^{2} \int_{-\infty}^{t} dt' \int_{-\infty}^{t'} dt'' H_{\text{int}}(t') H_{\text{int}}(t'').$$
(2.8)

By substituting this into Eq. (2.6), we obtain the transition probability per unit time with $t_0 \rightarrow \infty$,

 $W(q_f\alpha_f;q_i\alpha_i)$ in the following form:

$$W(q_{f}\alpha_{f}; q_{i}\alpha_{i})$$

$$= \int_{-\infty}^{0} dt \int_{-\infty}^{\infty} du' \int_{-\infty}^{u'} dt' \sum_{f'} \sum_{n,n'} \langle \Phi_{i} | H_{\text{int}}(t') | n' \rangle$$

$$\times \langle n' | H_{\text{int}}(u') | \Phi_{f'} \rangle \langle \Phi_{f'} | H_{\text{int}}(u) | n \rangle \langle n | H_{\text{int}}(t) | \Phi_{i} \rangle$$

$$= 2\pi \sum_{f'} \left| \sum_{n} \langle f | H_{\text{int}} | n \rangle \frac{1}{E_{g} + \omega_{i} - E_{n}} \langle n | H_{\text{int}} | \Phi_{i} \rangle \right|^{2}$$

$$\times \delta(E_{g} + \omega_{i} - E_{f'} - \omega_{f}), \qquad (2.9)$$

with $q_i \equiv (\mathbf{q}_i, \omega_i)$, $q_f \equiv (\mathbf{q}_f, \omega_f)$, and $|\Phi_{f'}\rangle = c_{q_f\alpha_f}|f'\rangle$. This is nothing but conventional expression of the second-order dipole allowed process, on which our following analysis is based. The $|f'\rangle$ represents the eigenstate of the Hamiltonian of the matter with the eigenvalue $E_{f'}$, while $|n\rangle$ represents the eigenstate with eigenvalue E_n in the presence of core hole.

In our previous paper having discussed RIXS at the Cu K edge, 25 the E1 transition could not directly change the 3d states but simply create the core-hole potential which attracts electrons in the 3d states. In such a situation, by treating the core-hole potential as a perturbation, we could conveniently introduce the Green functions and diagrams on the basis of the Keldysh-Schwinger formalism to calculate $W(q_f\alpha_f;q_i\alpha_i)$. To the present case, however, such diagrammatic procedure is difficult to apply, since the E1 transition modifies the 3d states from the $3d^9$ -configuration to the $3d^{10}$ -configuration, which change is hard to express by the diagrams for magnon excitations.

III. MAGNON EXCITATIONS AROUND THE CORE-HOLE SITE

A. General consideration

Assuming that the core hole is created at the origin in the intermediate state, we analyze the spin system around the origin, as shown in Fig. 2. We write the ground state $|g\rangle$ of $H_{\rm mag}$ as

$$|g\rangle = |\uparrow\rangle|\psi_0^{\uparrow}\rangle + |\downarrow\rangle|\psi_0^{\downarrow}\rangle, \tag{3.1}$$

where $|\uparrow\rangle$ and $|\downarrow\rangle$ represent the spin states at the origin, and $|\psi_0^{\uparrow}\rangle$ and $|\psi_0^{\downarrow}\rangle$ are constructed by the bases of the rest of spins. The expectation value of S^z at the origin may be expressed as

$$\langle S_0^{z'} \rangle = \frac{1}{2} \left\{ \langle \psi_0^{\uparrow} | \psi_0^{\uparrow} \rangle - \langle \psi_0^{\downarrow} | \psi_0^{\downarrow} \rangle \right\}. \tag{3.2}$$

Since the spin degree of freedom is lost at the origin just after the E1 transition takes place, the wave function becomes

$$H_{
m int}|g
angle \propto \sum_{m} \left[\sum_{\sigma=\uparrow,\downarrow} D^{lpha_i}(jm,\sigma) |\psi_0^{\sigma}
angle
ight] |jm
angle, \quad (3.3)$$

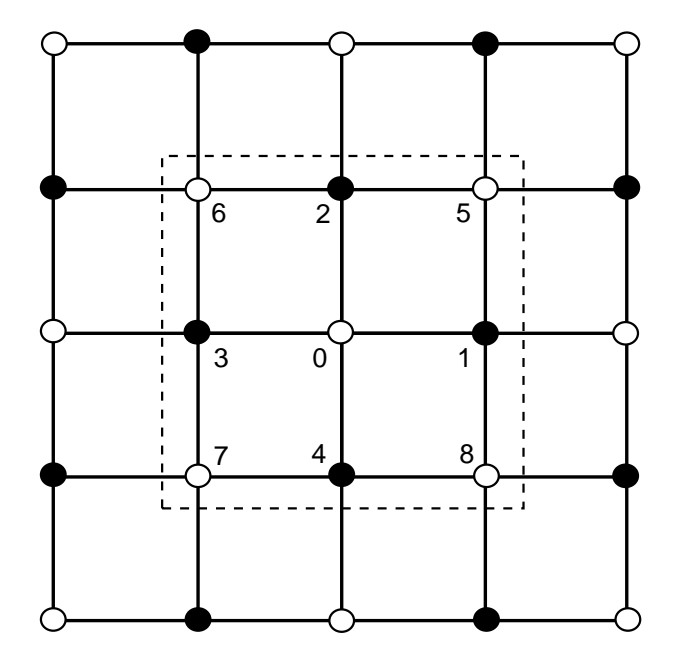


FIG. 2: Spins near the core-hole. Each site is labeled by number and the core-hole site is assigned number 0.

where $|jm\rangle$ represents the core hole state. Let H' be the Hamiltonian in the intermediate state. It consists of the exchange interaction terms excluding those with the core-hole site. The Hilbert space representing H' is different from the initial state. This situation is the same as the problem of the non-magnetic impurity. ^{39,40} Note that the states $|\psi_0^{\uparrow}\rangle$ and $|\psi_0^{\downarrow}\rangle$ are not the eigenstates of H'. They are expanded in terms of normalized eigenstate $|\phi_\eta\rangle$'s of H' with eigenvalue ϵ'_n . We therefore have

$$\sum_{n} H_{\text{int}} |n\rangle \frac{1}{\omega_{i} + E_{g} - E_{n}} \langle n|H_{\text{int}}|\Phi_{i}\rangle$$

$$\propto \sum_{m,\sigma,\sigma'} D^{\alpha_{f}} (jm,\sigma)^{*} D^{\alpha_{i}} (jm,\sigma')$$

$$\times \sum_{n} |\sigma\rangle |\phi_{\eta}\rangle R(\epsilon'_{\eta}) \langle \phi_{\eta}|\psi_{0}^{\sigma'}\rangle, \tag{3.4}$$

with

$$R(\epsilon'_{\eta}) = \frac{1}{\omega_i + \epsilon_g - \epsilon_{\text{core}} + i\Gamma - \epsilon'_{\eta}}, \quad (3.5)$$

where ϵ_g represents the ground state energy of $H_{\rm mag}$. The $\epsilon_{\rm core}$ denotes the energy required to create a core hole in the state $|jm\rangle$ and the $3d^{10}$ -configuration. The Γ stands for the life-time broadening width of the core hole; $\Gamma \sim 0.3$ eV at the L_3 edge. Since H' is different from $H_{\rm mag}$ only around the core-hole site, $|\phi_{\eta}\rangle$ could have sufficient overlap with $|\psi_0^{\sigma'}\rangle$ only when $\epsilon'_{\eta} - \epsilon_g$ varies in the range of several J's ($J \sim 0.1$ eV). Note that the spin degree of freedom at the origin is recovered in the final state and the wave function is given by $|\sigma\rangle|\phi_{\eta}\rangle$. The first

factor in Eq. (3.4) has relations,

$$\sum_{m} D^{\alpha_f}(jm,\sigma)^* D^{\alpha_i}(jm,\sigma) \equiv P_{\sigma}^{(0)}(j;\alpha_f,\alpha_i)(3.6)$$

$$\sum_{m} D^{\alpha_f}(jm,\sigma)^* D^{\alpha_i}(jm,-\sigma) \equiv P_{\sigma}^{(1)}(j;\alpha_f,\alpha_i)(3.7)$$

Here, for $\sigma=\uparrow$, $-\sigma$ denotes \downarrow , and vice versa. Table II shows $P_{\sigma}^{(0)}$ and $P_{\sigma}^{(1)}$ for α_i and α_f along the x,y, and z axes. The extension to the cases of general α_i and α_f directions is obvious. The $P_{\sigma}^{(0)}$ and $P_{\sigma}^{(1)}$ correspond to the spin-conserving and the spin-flip processes, respectively. Note that $P_{\sigma}^{(1)}(1/2;\alpha_f,\alpha_i)+P_{\sigma}^{(1)}(3/2;\alpha_f,\alpha_i)=0$. As will become clear later, spin-flip excitation spectra are proportional to $|P^{(1)}|^2$. Therefore, if the processes for j=3/2 and j=1/2 are not separated, no spin-flip excitation comes out.

B. Scattering channel with changing the polarization

We analyze the scattering channel that the polarization changes; let α_i and α_f be along y and x axes, respectively. We assume that the staggered magnetic moment is parallel to the z'-axis, where the coordinate frame of the x', y', z' axes is specified by the Euler angles α , β , and γ from the coordinate frame of the x, y, z axes. We have the spin-conserving term coming from $P_{\sigma}^{(0)}$ and the spin-flipping term coming from $P_{\sigma}^{(1)}$. The spin-conserving term is given by

$$\sum_{n} H_{\text{int}} | n \rangle \frac{1}{\omega_{i} + E_{g} - E_{n}} \langle n | H_{\text{int}} | g \rangle$$

$$\propto P_{\uparrow}^{(0)} | \uparrow \rangle \sum_{\eta} |\phi_{\eta}\rangle R(\epsilon'_{\eta}) \langle \phi_{\eta} | \psi_{0}^{\uparrow} \rangle$$

$$+ P_{\downarrow}^{(0)} | \downarrow \rangle \sum_{\eta} |\phi_{\eta}\rangle R(\epsilon'_{\eta}) \langle \phi_{\eta} | \psi_{0}^{\downarrow} \rangle,$$

$$\propto \left(-\frac{i}{15} \right) \cos \beta \left\{ | \uparrow \rangle \sum_{\eta} |\phi_{\eta}\rangle R(\epsilon'_{\eta}) \langle \phi_{\eta} | \psi_{0}^{\uparrow} \rangle$$

$$- | \downarrow \rangle \sum_{\eta} |\phi_{\eta}\rangle R(\epsilon'_{\eta}) \langle \phi_{\eta} | \psi_{0}^{\downarrow} \rangle \right\}.$$
(3.8)

Since this state has an overlap to the ground state, we have the elastic amplitude $A_{\rm elas},$

$$A_{\text{elas}} \propto \left(-\frac{i}{15}\right) \cos \beta \left\{ \langle \psi_0^{\uparrow} | \sum_{\eta} |\phi_{\eta} \rangle R(\epsilon_{\eta}') \langle \phi_{\eta} | \psi_0^{\uparrow} \rangle - \langle \psi_0^{\downarrow} | \sum_{\eta} |\phi_{\eta} \rangle R(\epsilon_{\eta}') \langle \phi_{\eta} | \psi_0^{\downarrow} \rangle \right\}.$$
(3.9)

Introducing the quantity

$$f_{\sigma}^{(1)}(\omega_i) = \frac{1}{\langle \psi_0^{\sigma} | \psi_0^{\sigma} \rangle} \langle \psi_0^{\sigma} | \sum_{\eta} |\phi_{\eta}\rangle R(\epsilon_{\eta}') \langle \phi_{\eta} | \psi_0^{\sigma} \rangle, \quad (3.10)$$

		$P_{\sigma}^{(0)}$			$P_{\sigma}^{(1)}$		
\overline{j}	$\alpha_f \setminus \alpha_i$	x	y	z	x	y	z
3/2	x	2 15	$\mp \frac{i}{15} \cos \beta$	0	0	$\frac{i}{15}e^{\pm i\gamma}\sin\beta$	0
-	y	$\pm \frac{i}{15} \cos \beta$	2 15	0	$-\frac{i}{15}e^{\pm i\gamma}\sin\beta$	0	0
	\overline{z}	0	0	0	0	0	0
$\frac{1}{2}$	x	1 15	$\pm \frac{i}{15} \cos \beta$	0	0	$-\frac{i}{15}e^{\pm i\gamma}\sin\beta$	0
-	y	$\mp \frac{i}{15} \cos \beta$	1 15	0	$\frac{i}{15}e^{\pm i\gamma}\sin\beta$	0	0
	z	0	0	0	0	0	0

TABLE II: $P_{\sigma}^{(0)}(j; \alpha_f, \alpha_i)$ and $P_{\sigma}^{(1)}(j; \alpha_f, \alpha_i)$ where upper and lower signs correspond to $\sigma = \uparrow$ and \downarrow , respectively.

with $\sigma = \uparrow$ and \downarrow , we define $f_0^{(1)}(\omega_i)$ and $\Delta(\omega_i)$ by

$$f_{\sigma}^{(1)}(\omega_i) = f_0^{(1)}(\omega_i) \pm \frac{1}{2}\Delta(\omega_i),$$
 (3.11)

where plus and minus signs in the second term correspond to $\sigma = \uparrow$ and \downarrow , respectively. In the far-off-resonance condition that $\omega_i \ll \epsilon_{\rm core}$ or $\omega_i \gg \epsilon_{\rm core}$, and in the large limit of Γ , which is called as the UCL condition, that $\Gamma \gg |\omega_i - \epsilon_{\rm core}|, |\epsilon'_{\eta} - \epsilon_{g}|$, we could factor out $R(\epsilon'_{\eta})$ from the summation over η in Eq. (3.10). Thereby, using $\sum_{\eta} |\phi_{\eta}\rangle\langle\phi_{\eta}| = 1$, we immediately obtain $\Delta(\omega_i) = 0$.

By inserting Eq. (3.11) in Eq. (3.9), and by using Eq. (3.2), we have

$$A_{\rm elas} \propto \left(-\frac{i}{15}\right) \cos \beta \left\{ 2f_0^{(1)}(\omega_i) \langle S_0^{z'} \rangle + \frac{1}{2}\Delta(\omega_i) \right\}.$$
 (3.12)

This result may be compared with the conventional expression of the elastic magnetic scattering amplitude by Hannon $et\ al.$, ⁴²

$$\sigma^{(1)}\boldsymbol{\alpha}_f \times \boldsymbol{\alpha}_i \cdot \mathbf{m}, \tag{3.13}$$

where **m** is the staggered magnetic moment vector, and $\sigma^{(1)}$ is a certain numerical constant. In order that Eq. (3.12) is consistent with Eq. (3.13), $\Delta(\omega_i)$ could be, if it existed, expanded as $a \sum_{\delta} \langle S_{\delta}^{z'} \rangle + b \sum_{\delta'} \langle S_{\delta'}^{z'} \rangle + \cdots$ with δ and δ' denoting the nearest and next nearest neighbor sites to the core-hole site 0 (a and b have to go to zero in the far-off-resonance condition as well as in the UCL condition), since $\Delta(\omega_i)$ should be incorporated into the renormalization of $\sigma^{(1)}$ in Eq. (3.13). The presence of $\Delta(\omega_i)$ may suggest that the disturbance through the intermediate state reaches to the neighboring lattice sites. Actually, Eq. (3.8) has finite overlaps to $S_{\delta}^{z'}|g\rangle$ and $S_{\delta'}^{z'}|g\rangle$, which are not orthogonal to both $S_0^{z'}|g\rangle$ and $S_0^{z'}|g\rangle$. By neglecting such possibility, we project Eq. (3.8) onto $|g\rangle$ and $S_0^{z'}|g\rangle$. Since $S_0^{z'}|g\rangle$ is not orthogonal to $|g\rangle$ and not normalized, we need to introduce overlap matrix $\hat{\rho}$ between $|g\rangle$ and $S_0^{z'}|g\rangle$. Using the inverse of $\hat{\rho}$, we have

$$\sum_{n} H_{\text{int}} |n\rangle \frac{1}{\omega_{i} + E_{g} - E_{n}} \langle n|H_{\text{int}}|g\rangle$$

$$= \left(-\frac{i}{15}\right) \cos\beta \left\{\frac{1}{2}\Delta(\omega_{i})|g\rangle + 2f_{0}^{(1)}(\omega_{i})S_{0}^{z'}|g\rangle (3.14)\right\}$$

By neglecting $\Delta(\omega_i)$, the final state in this channel is approximated as

$$\left(-\frac{i}{15}\right)\cos\beta 2f_0^{(1)}(\omega_i)S_0^{z'}|g\rangle
= \left(-\frac{i}{15}\right)2f_0^{(1)}(\omega_i)\boldsymbol{\alpha}_{f\perp}\times\boldsymbol{\alpha}_{i\perp}\cdot\mathbf{S}_{0\parallel}|g\rangle, (3.15)$$

where $\mathbf{S}_{0\parallel}$ stands for the component of \mathbf{S}_0 parallel to the direction of the staggered magnetic moment. The $\boldsymbol{\alpha}_{i\perp}$ and $\boldsymbol{\alpha}_{f\perp}$ represent the polarization vectors projected onto the x-y plane. Therefore $\boldsymbol{\alpha}_{f\perp} \times \boldsymbol{\alpha}_{i\perp}$ is always parallel to the z axis. Note that the inelastic terms are sometimes inferred from Eq. (3.13) with simply replacing \mathbf{m} by the spin operator \mathbf{S}_0 at site 0.⁴³ Equation (3.15) is, however, different from such a term, since Eq. (3.15) is restricted within the spin-conserving process, and disappears for $\beta = \pi/2$.

The final states responsible to inelastic scattering mainly come from the spin-flip terms,

$$\sum_{n} H_{\text{int}} |n\rangle \frac{1}{\omega_{i} + E_{g} - E_{n}} \langle n|H_{\text{int}}|\Phi_{i}\rangle$$

$$\propto P_{\downarrow}^{(1)} |\downarrow\rangle \sum_{\eta} |\phi_{\eta}\rangle R(\epsilon'_{\eta}) \langle \phi_{\eta}|\psi_{0}^{\downarrow}\rangle$$

$$+ P_{\uparrow}^{(1)} |\uparrow\rangle \sum_{\eta} |\phi_{\eta}\rangle R(\epsilon'_{\eta}) \langle \phi_{\eta}|\psi_{0}^{\uparrow}\rangle,$$

$$\propto \left(\frac{i}{15}\right) \sin\beta \left\{ e^{-i\gamma} |\downarrow\rangle \sum_{\eta} |\phi_{\eta}\rangle R(\epsilon'_{\eta}) \langle \phi_{\eta}|\psi_{0}^{\uparrow}\rangle$$

$$+ e^{i\gamma} |\uparrow\rangle \sum_{\eta} |\phi_{\eta}\rangle R(\epsilon'_{\eta}) \langle \phi_{\eta}|\psi_{0}^{\downarrow}\rangle \right\}.$$
(3.16)

We project this state onto $S_0^{\pm}|g\rangle$ with $S_0^{\pm}=S_0^{x'}\pm iS_0^{y'}$. These states are orthogonal to each other and to $|g\rangle$ but not normalized, that is, $\langle g|S_0^-S_0^+|g\rangle=\langle \psi_0^{\downarrow}|\psi_0^{\downarrow}\rangle$ and $\langle g|S_0^+S_0^-|g\rangle=\langle \psi_0^{\uparrow}|\psi_0^{\uparrow}\rangle$. Thereby we could express Eq. (3.16) as

$$\propto \left(\frac{i}{15}\right) \sin \beta \left\{ f_0^{(1)}(\omega_i) (e^{-i\gamma} S_0^- + e^{i\gamma} S_0^+) |g\rangle + \frac{1}{2} \Delta(\omega_i) (e^{-i\gamma} S_0^- - e^{i\gamma} S_0^+) |g\rangle \right\}.$$
(3.17)

The first term may be rewritten as

$$\left(\frac{i}{15}\right) \sin \beta 2 f_0^{(1)}(\omega_i) \left(\cos \gamma S_0^{x'} - \sin \gamma S_0^{y'}\right) |g\rangle
= \left(-\frac{i}{15}\right) 2 f_0^{(1)}(\omega_i) \boldsymbol{\alpha}_{f\perp} \times \boldsymbol{\alpha}_{i\perp} \cdot \mathbf{S}_{0\perp} |g\rangle,$$
(3.18)

where $\mathbf{S}_{0\perp}$ represents the component perpendicular to the direction of the staggered magnetic moment. As regards the second term of Eq. (3.17), the inclusion of $\Delta(\omega_i)$ would require adding the states $S_{\delta}^{\pm}|g\rangle$ and $S_{\delta'}^{\pm}|g\rangle$ as the states to be projected. Such an analysis would be rather complicated and will not be attempted in this paper. With disregarding the term of $\Delta(\omega_i)$, we finally have the expression of the final state by combining Eq. (3.15) with Eq. (3.17);

$$\sum_{n} H_{\text{int}}|n\rangle \frac{1}{\omega_{i} + E_{g} - E_{n}} \langle n|H_{\text{int}}|g\rangle = 2f_{0}^{(1)}(\omega_{i})\alpha_{f} \times \alpha_{i} \cdot \mathbf{S}_{0}|g\rangle$$
(3.19)

C. Scattering channel without changing the polarization

In this scattering channel, only the spin-conserving excitations are brought about through the diagonal components of $P_{\sigma}^{(0)}$. For $\alpha_i = \alpha_f = (1,0,0)$ and for $\alpha_i = \alpha_f = (0,1,0)$, we have

$$\sum_{n} H_{\text{int}} |n\rangle \frac{1}{\omega_{i} + E_{g} - E_{n}} \langle n|H_{\text{int}}|g\rangle$$

$$\propto \left(\frac{2}{15}\right) \left\{ |\uparrow\rangle \sum_{\eta} |\phi_{\eta}\rangle R(\epsilon'_{\eta}) \langle \phi_{\eta}|\psi_{0}^{\uparrow}\rangle + |\downarrow\rangle \sum_{\eta} |\phi_{\eta}\rangle R(\epsilon'_{\eta}) \langle \phi_{\eta}|\psi_{0}^{\downarrow}\rangle \right\}. \tag{3.20}$$

We consider the spherical form of the final state, $\mathbf{X} \cdot \mathbf{S}_0 | g \rangle$ with $\mathbf{X} \equiv \sum_{\delta} \mathbf{S}_{\delta}$. The deviation from the spherical form would be considered as a next-step approximation, since we are neglecting $\Delta(\omega_i)$ which suggests that $\mathbf{S}_{\delta} | g \rangle$ are to be included as possible excited states. Since $\mathbf{X} \cdot \mathbf{S}_0 | g \rangle$ is not orthogonal to $| g \rangle$, we introduce the overlap matrix $\hat{\rho}$ defined by $(\hat{\rho})_{i,j} \equiv \langle \psi_i | \psi_j \rangle$ with $| \psi_1 \rangle \equiv | g \rangle$ and $| \psi_2 \rangle \equiv \mathbf{X} \cdot \mathbf{S}_0 | g \rangle$. Then, using the inverse of $\hat{\rho}$, we project the final state onto these states, resulting that

$$\sum_{n} H_{\text{int}} |n\rangle \frac{1}{\omega_{i} + E_{g} - E_{n}} \langle n|H_{\text{int}}|g\rangle$$

$$\propto f_{1}^{(2)}(\omega_{i})|g\rangle + f_{2}^{(2)}(\omega_{i})\mathbf{X} \cdot \mathbf{S}_{0}|g\rangle \tag{3.21}$$

where $f_m^{(2)}(\omega_i)$'s are given by

$$f_m^{(2)}(\omega_i) = \sum_{m'} (\hat{\rho}^{-1})_{m,m'} Q_{m'}^{(2)}(\omega_i), \qquad (3.22)$$

with

$$Q_{1}^{(2)}(\omega_{i}) = \sum_{\sigma} \langle \psi_{0}^{\sigma} | \sum_{\eta} |\phi_{\eta}\rangle R(\epsilon_{\eta}^{\prime}) \langle \phi_{\eta} | \psi_{0}^{\sigma} \rangle, \qquad (3.23)$$

$$Q_{2}^{(2)}(\omega_{i}) = \frac{1}{2} \Big\{ \sum_{\sigma} \operatorname{sgn}(\sigma) \langle \psi_{0}^{\sigma} | X^{z^{\prime}} \sum_{\eta} |\phi_{\eta}\rangle R(\epsilon_{\eta}^{\prime}) \langle \phi_{\eta} | \psi_{0}^{\sigma} \rangle + \langle \psi_{0}^{\uparrow} | X^{-} \sum_{\eta} |\phi_{\eta}\rangle R(\epsilon_{\eta}^{\prime}) \langle \phi_{\eta} | \psi_{0}^{\downarrow} \rangle + \langle \psi_{0}^{\downarrow} | X^{+} \sum_{\eta} |\phi_{\eta}\rangle R(\epsilon_{\eta}^{\prime}) \langle \phi_{\eta} | \psi_{0}^{\uparrow} \rangle \Big\}, \qquad (3.24)$$

where $sgn(\sigma) = 1$ for $\sigma = \uparrow$ and -1 for $\sigma = \downarrow$.

To understand the possible spin-flip at the origin in Eq. (3.21), we take up the second term of Eq. (3.24), and examine the associated generating process. Consider that the down spin at the core-hole site is annihilated by absorbing photon. The wave function for surrounding spins is expressed by $|\psi_0^{\downarrow}\rangle$, which satisfies $\langle\psi_0^{\downarrow}|(\sum_i S_i^z)|\psi_0^{\downarrow}\rangle=1/2$ with i running all the lattice sites except the origin. At the end of time evolution in the intermediate state, this wave function is modified, and could have a finite overlap with the state $X^+|\psi_0^{\uparrow}\rangle$, since $\langle\psi_0^{\uparrow}|X^-(\sum_i S_i^{z'})X^+|\psi_0^{\uparrow}\rangle=1/2$. Then, the 3d hole with down spin is created at the core-hole site by annihilating the core hole with emitting photon, leading to $|\downarrow\rangle X^+|\psi_0^{\uparrow}\rangle$. Since $S_0^-|g\rangle=|\downarrow\rangle|\psi_0^{\uparrow}\rangle$, this state is nothing but $X^+S_0^-|g\rangle$.

In the far-off-resonance condition and in the UCL approximation, $R(\epsilon'_{\eta})$ could be factored out in Eqs. (3.23) and (3.24). It leads to $Q_m(\omega_i) = R(\epsilon'_0)(\hat{\rho})_{m,1}$ and as a consequence,

$$f_m^{(2)}(\omega_i) = R(\epsilon_0') \sum_{m'} (\hat{\rho}^{-1})_{m,m'} (\hat{\rho})_{m',1} = R(\epsilon_0') \delta_{m,1}.$$
(3.25)

Therefore, in both cases, the spin-conserving excitations could not be generated.

One may formally write the intermediate state Hamiltonian H' by eliminating the bonds which connect the spin at the origin to spins at neighboring sites from the initial state Hamiltonian H_{mag} :

$$H' = H_{\text{mag}} + V, \quad V = -J \sum_{\delta} \mathbf{S}_0 \cdot \mathbf{S}_{\delta}.$$
 (3.26)

The Hilbert space representing Eq. (3.26) formally contains the spin-degrees of freedom at the core-hole site, which should be completely decoupled from the outer spins in the final solution, as known from the non-magnetic impurity problem. 39,40 Finite-order perturbation with V could not satisfy this criteria. In this context, although a first-order perturbation with V has been attempted to include two-magnon excitations by extending the UCL approximation, 41 it may be logically inappropriate.

D. Cluster model

It is not easy to evaluate accurately $f_0^{(1)}(\omega_i)$ and $f_m^{(2)}(\omega_i)$'s. In this paper, we use a cluster consisting of a central spin and of 8 neighboring spins, as shown in Fig. 2. The outer spins labeled as $\mathbf{S}_1 \sim \mathbf{S}_8$ are assumed under the staggered field from spins outside the cluster. For the central spin \mathbf{S}_0 belonging to the A sublattice, the initial-state Hamiltonian is given by

$$H_{\text{mag}} = J \sum_{\langle i,j \rangle} \mathbf{S}_i \cdot \mathbf{S}_j + \frac{J}{2} \sum_{i=1}^4 S_i^z - 2\frac{J}{2} \sum_{j=5}^8 S_j^z, \quad (3.27)$$

which is represented by the matrix with 512×512 dimensions. The intermediate-state Hamiltonian is given just by eliminating \mathbf{S}_0 from Eq. (3.27), which is represented by the matrix with 256×256 dimensions. Diagonalizing numerically the Hamiltonian matrices, we obtain the eigenstates of $H_{\rm mag}$ and H'. We obtain, for example, $\langle S_0^z \rangle = 0.394$ from Eq. (3.2). This value is an overestimate of the sublattice magnetization in comparison with the 1/S-expansion value in second order $0.307,^{30}$ probably due to the finite-size effect. Using the eigenstates of $H_{\rm mag}$ and H', we evaluate $f_0^{(1)}$ from Eqs. (3.10) and (3.11), and $f_m^{(2)}$ from Eqs. (3.23) and (3.24). Since the cluster size is strongly subject to the boundary, the values thus obtained may be considered as a semi-quantitative estimate.

Using the notation in the preceding subsection, we express the $L_{2,3}$ -absorption coefficient $A_i(\omega_i)$,

$$A_{j}(\omega_{i}) = \sum_{\alpha_{i}} P^{(0)}(j; \alpha_{i}, \alpha_{i}) \sum_{\sigma, \eta} |\langle \phi_{\eta} | \psi_{0}^{\sigma} \rangle|^{2}$$

$$\times \frac{\Gamma/\pi}{(\omega_{i} + \epsilon_{g} - \epsilon_{\text{core}} - \epsilon_{\eta}^{\prime})^{2} + \Gamma^{2}}.$$
 (3.28)

Substituting the eigenstates of the cluster model into Eq. (3.28), we calculate $A_j(\omega_i)$. Figure 3 shows the calculated $A_j(\omega_i)$ as a function of photon energy. The origin of photon energy is $\omega_i = \epsilon_{\rm core}$. The dimensionless life-time broadening width of the core hole is chosen as $\Gamma/(2J) = 1.2$. The calculated curve is found very close to the Lorentzian shape. By comparison with the experimental curve for the Cu L_3 -edge in ${\rm Sr}_2{\rm CuO}_2{\rm Cl}_2$, Γ is estimated $\sim 2.4J$ with J=130 meV.

E. Spin correlation function

The core hole could be excited at all the Cu sites in the x-ray scattering event. For the contribution from the core-hole site \mathbf{r}_{ℓ} , we need to multiply weight $\exp(i\mathbf{q} \cdot \mathbf{r}_{\ell})$ ($\mathbf{q} \equiv \mathbf{q}_i - \mathbf{q}_f$) to the amplitudes discussed in the preceding subsections. Collecting the contributions from each corehole site in Eq. (2.9), we finally obtain the expression of

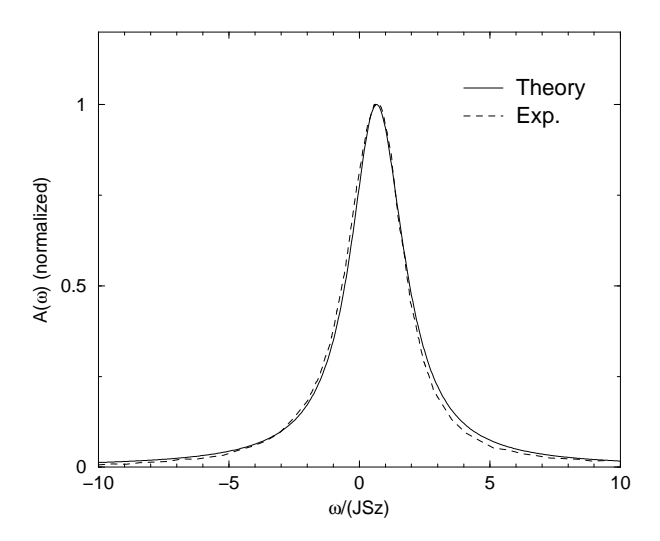


FIG. 3: Absorption coefficient $A(\omega_i)$ as a function of photon energy ω_i . $\Gamma/(2J)=1.2$. The origin of energy is set to correspond to $\omega_i=\epsilon_{\rm core}$. The dotted line represents the XAS experimental data at the Cu L_3 edge in Sr₂CuO₂Cl₂, ³⁵ where J is assumed to be 130 meV, and the experimental curve is shifted such that the peak position coincides with the calculation.

the RIXS spectra:

$$W(q_f \alpha_f; q_i \alpha_i) = \frac{w^4}{4\omega_i \omega_f} \Big\{ |P^{(1)}(j; \alpha_f, \alpha_i)|^2 Y^{(1)}(\omega_i; \mathbf{q}, \omega) + |P^{(0)}(j; \alpha_f, \alpha_i)|^2 Y^{(2)}(\omega_i; \mathbf{q}, \omega) \Big\}, (3.29)$$

where the spin-flip and the spin-conserving correlation functions are defined by

$$Y^{(1)}(\omega_i; \mathbf{q}, \omega) = \int_{-\infty}^{\infty} \langle Z^{(1)\dagger}(\omega_i; \mathbf{q}, t) Z^{(1)}(\omega_i; \mathbf{q}, 0) \rangle e^{i\omega t} dt,$$
(3.30)

$$Y^{(2)}(\omega_i; \mathbf{q}, \omega) = \int_{-\infty}^{\infty} \langle Z^{(2)\dagger}(\omega_i; \mathbf{q}, t) Z^{(2)}(\omega_i; \mathbf{q}, 0) \rangle e^{i\omega t} dt,$$
(3.31)

where the angular bracket denotes the expectation value in the ground state. Operators $Z^{(1)}(\omega_i; \mathbf{q})$ and $Z^{(2)}(\omega_i; \mathbf{q})$ are given by

$$Z^{(1)}(\omega_{i}; \mathbf{q}) = 2f_{0}^{(1)}(\omega_{i}) \left\{ S_{a}^{x'}(-\mathbf{q}) + S_{b}^{x'}(-\mathbf{q}) \right\}$$
(3.32)

$$Z^{(2)}(\omega_{i}; \mathbf{q}) = f_{2}^{(2)}(\omega_{i}) \left\{ (X^{z'}S^{z'})_{a}(-\mathbf{q}) + (X^{z'}S^{z'})_{b}(-\mathbf{q}) + (X^{x'}S^{x'})_{a}(-\mathbf{q}) + (X^{x'}S^{x'})_{b}(-\mathbf{q}) + (X^{y'}S^{y'})_{a}(-\mathbf{q}) + (X^{y'}S^{y'})_{b}(-\mathbf{q}) \right\}.$$
(3.33)

The Fourier transforms of $S_0^{x'}$ and $X^{x'(y',z')}S_0^{x'(y',z')}$ are defined separately for the A and B sublattices and discriminated by subscripts a and b, respectively. For ex-

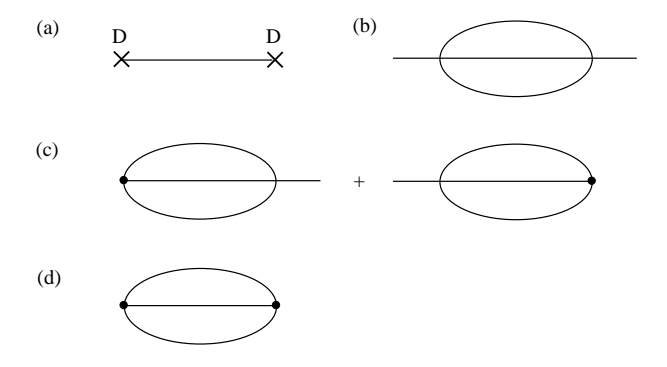


FIG. 4: Diagrams for the time-ordered Green function $\tilde{Y}^{(1)}(\omega_i; \mathbf{q}, \omega)$ required to evaluate the correction up to the $1/(2S)^2$. Solid lines represent the unperturbed Green functions $G_{\alpha\alpha}^{(0)}(\mathbf{k},\omega)$ or $G_{\beta\beta}^{(0)}(\mathbf{k},\omega)$, on which the arrows and the type $(\alpha \text{ or } \beta)$ are omitted. The crosses in diagram (a) represent the spin reduction factor. Solid circles represent the three-magnon terms given by Eq. (4.1) and their Hermitian conjugates.

ample, by multiplying weight $e^{i\mathbf{q}\cdot\mathbf{r}_{\ell}}$, we have

$$(X^{x'}S^{x'})_a(-\mathbf{q}) = \sum_{i \in A} \frac{1}{2} \sum_{\delta} S_{i+\delta}^{x'} S_i^{x'} e^{i\mathbf{q} \cdot \mathbf{r}_i}, (3.34)$$

$$(X^{x'}S^{x'})_b(-\mathbf{q}) = \sum_{j \in \mathbf{B}} \frac{1}{2} \sum_{\delta} S_{j+\delta}^{x'} S_j^{x'} e^{i\mathbf{q} \cdot \mathbf{r}_j}.$$
 (3.35)

Note that $Y^{(1)}(\omega_i; \mathbf{q}, \omega)$ is proportional to the dynamical structure factor of the transverse spin, while

 $Y^{(2)}(\omega_i; \mathbf{q}, \omega)$ is proportional to the "exchange"-type spin-spin correlation function discussed in the magnetic excitations in the K-edge RIXS.^{11,25}

IV. SPIN CORRELATION FUNCTION WITHIN THE 1/S EXPANSION

Spin-flip and spin-conserving excitations derived in the preceding section could freely propagate in the crystal in the final state because of the absence of core hole. Therefore, the cluster model with small size would not work well in the final state. We exploit the 1/S-expansion method in the study of the final state. Notations and several relations required in the present study are briefly summarized in Appendix.

A. Spin-flip excitation spectra

We express the spin-flip operator $Z^{(1)}(\omega_i; \mathbf{q})$ in terms of magnon operators by using Eqs. (A1)-(A10). Since $Z^{(1)}(\omega_i; \mathbf{q})$ is proportional to $S_a^{x'}(-\mathbf{q}) + S_b^{x'}(-\mathbf{q})$, the derivation is parallel to those of Eqs. (6.9) and (6.10) in Ref. 45 in the study of the dynamical structure factor. In the following, we simply write down the result.

For \mathbf{q} being inside the first magnetic Brillouin zone (MBZ), we have

$$Z^{(1)}(\omega_{i}; \mathbf{q}) = \sqrt{\frac{N}{2}} \sqrt{2S} \frac{1}{2} f_{0}^{(1)}(\omega_{i}) (\ell_{\mathbf{q}} + m_{\mathbf{q}}) \left[D(\alpha_{-\mathbf{q}}^{\dagger} + \beta_{-\mathbf{q}}^{\dagger}) + (\alpha_{\mathbf{q}} + \beta_{\mathbf{q}}) \right]$$

$$- \frac{1}{2S} \frac{2}{N} \sum_{234} \delta_{\mathbf{G}}(\mathbf{q} + 2 - 3 - 4) \frac{1}{2} \ell_{\mathbf{q}} \ell_{2} \ell_{3} \ell_{4}$$

$$\times \left\{ M_{\mathbf{q}234}^{(1)} + \operatorname{sgn}(\gamma_{\mathbf{G}}) M_{\mathbf{q}234}^{(2)} \right\} \left\{ \beta_{2}^{\dagger} \alpha_{-3}^{\dagger} \alpha_{-4}^{\dagger} + \beta_{-2} \alpha_{3} \alpha_{4} + \operatorname{sgn}(\gamma_{\mathbf{G}}) \left(\alpha_{2}^{\dagger} \beta_{-3}^{\dagger} \beta_{-4}^{\dagger} + \alpha_{-2} \beta_{3} \beta_{4} \right) \right\} \right], (4.1)$$

where

$$M_{\mathbf{q}234}^{(1)} = -x_2 + \operatorname{sgn}(\gamma_{\mathbf{G}})x_{\mathbf{q}}x_3x_4,$$
 (4.2)

$$M_{\mathbf{q}234}^{(2)} = x_3 x_4 - \operatorname{sgn}(\gamma_{\mathbf{G}}) x_{\mathbf{q}} x_2.$$
 (4.3)

The Kronecker delta $\delta_{\mathbf{G}}(\mathbf{q}+2-3-4)$ indicates the conservation of momenta within a reciprocal lattice vector \mathbf{G} and $\operatorname{sgn}(\gamma_{\mathbf{G}})$ denotes the sign of $\gamma_{\mathbf{G}}$. $x_{\mathbf{k}}$ is defined by Eq. (A11). The *spin reduction factor* D, which is related to the zero-point reduction of spin, is given by

$$D = 1 - \frac{\Delta S}{2S} - \frac{1}{4} \frac{\Delta S(1 + 3\Delta S)}{(2S)^2},$$
 (4.4)

with

$$\Delta S = \frac{1}{N} \sum_{\mathbf{k}} (\epsilon_{\mathbf{k}}^{-1} - 1). \tag{4.5}$$

For the square lattice, $\Delta S = 0.1966$.

Introducing the time-ordered Green function defined by $\tilde{Y}^{(1)}(\omega_i; \mathbf{q}, \omega) \equiv -i \int \langle T(Z^{(1)\dagger}(\omega_i; \mathbf{q}, t) Z^{(1)}(\omega_i; \mathbf{q}, 0) \rangle e^{i\omega t} dt$, we expand the Green function up to the second order with 1/S, which diagrams are shown in Fig. 4. We obtain the correlation function from the time-ordered Green function by the fluctuation-dissipation theorem, $Y^{(1)}(\omega_i; \mathbf{q}, \omega) = -2\text{Im}\tilde{Y}^{(1)}(\omega_i; \mathbf{q}, \omega)$. Here, ImX means

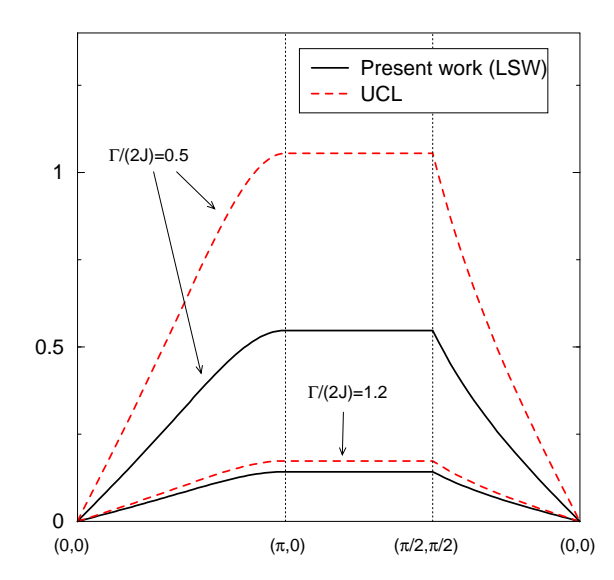


FIG. 5: (Color online) One-magnon intensity $y_1(\omega_i; \mathbf{q})/[N(2S)]$ within the LSW contribution, as a function of \mathbf{q} along symmetry lines, in comparison with the results of the UCL approximation (red broken line). The ω_i is set to give rise to the peak in the absorption spectra.

imaginary part of quantity X. The correlation function is found to consist of the δ -function peak of the one-magnon excitation and the continuum of three-magnon excitations, that is,

$$Y^{(1)}(\omega_i; \mathbf{q}, \omega) = y_1(\omega_i; \mathbf{q})(2\pi)\delta(\omega - \epsilon_{\mathbf{q}}) + y_3(\omega_i; \mathbf{q}, \omega).$$
(4.6)

Within the second-order of 1/S, the one-magnon spectral weight $y_1(\mathbf{q})$ may be expressed as

$$y_{1}(\omega_{i}; \mathbf{q}) = N(2S) |f_{1}^{(1)}(\omega_{i}) m_{\mathbf{q}} + f_{2}^{(1)}(\omega_{i}) \ell_{\mathbf{q}}|^{2} \times \left\{ 1 + \frac{1}{2S} y_{1,1}(\mathbf{q}) + \frac{1}{(2S)^{2}} y_{1,2}(\mathbf{q}) \right\}, (4.7)$$

where

$$y_{1,1}(\mathbf{q}) = (-2\Delta S),$$

$$y_{1,2}(\mathbf{q}) = -\frac{1}{2}\Delta S(1 + \Delta S) + \frac{-1}{\epsilon_{\mathbf{q}}} \sum_{\alpha\beta}^{(2)} (\mathbf{q}, \epsilon_{\mathbf{q}})$$

$$+ \left(\frac{2}{N}\right)^{2} \sum_{\mathbf{p}\mathbf{p}'} 2\ell_{\mathbf{q}}^{2} \ell_{\mathbf{p}}^{2} \ell_{\mathbf{p}'}^{2} \ell_{\mathbf{q}+\mathbf{p}-\mathbf{p}'}^{2} \left[\frac{-|B_{\mathbf{q},\mathbf{p},\mathbf{p}',[\mathbf{q}+\mathbf{p}-\mathbf{p}']}^{(4)}|^{2}}{(\epsilon_{\mathbf{q}} - \epsilon_{\mathbf{p}} - \epsilon_{\mathbf{p}'} - \epsilon_{\mathbf{q}+\mathbf{p}-\mathbf{p}'})^{2}} + \frac{|B_{\mathbf{q},\mathbf{p},\mathbf{p}',[\mathbf{q}+\mathbf{p}-\mathbf{p}']}^{(6)}|^{2}}{(\epsilon_{\mathbf{q}} + \epsilon_{\mathbf{p}} + \epsilon_{\mathbf{p}'} + \epsilon_{\mathbf{q}+\mathbf{p}-\mathbf{p}'})^{2}} \right]$$

$$+ \left(\frac{2}{N}\right)^{2} \sum_{\mathbf{p}\mathbf{p}'} 2\ell_{\mathbf{q}}^{2} \ell_{\mathbf{p}'}^{2} \ell_{\mathbf{k}+\mathbf{p}-\mathbf{p}'}^{2} \left[\frac{B_{\mathbf{q},\mathbf{p},\mathbf{p}',[\mathbf{q}+\mathbf{p}-\mathbf{q}']}^{(4)} N_{\mathbf{q},\mathbf{p},\mathbf{p}',[\mathbf{q}+\mathbf{p}-\mathbf{p}']}^{(1)}}{(\epsilon_{\mathbf{q}} - \epsilon_{\mathbf{p}} - \epsilon_{\mathbf{p}'} - \epsilon_{\mathbf{q}+\mathbf{p}-\mathbf{p}'})} - \frac{\operatorname{sgn}(\gamma_{\mathbf{G}}) B_{\mathbf{q},\mathbf{p},\mathbf{p}',[\mathbf{q}+\mathbf{p}-\mathbf{p}']}^{(6)} N_{\mathbf{q},\mathbf{p},\mathbf{p}',[\mathbf{q}+\mathbf{p}-\mathbf{p}']}^{(2)}}{\epsilon_{\mathbf{q}} + \epsilon_{\mathbf{p}} + \epsilon_{\mathbf{p}'} + \epsilon_{\mathbf{q}+\mathbf{p}-\mathbf{p}'}} \right].$$

$$(4.9)$$

with

$$N_{\mathbf{q},\mathbf{p},\mathbf{p}'[\mathbf{q}+\mathbf{p}-\mathbf{p}']}^{(1)} = M_{\mathbf{q},\mathbf{p},\mathbf{p}',[\mathbf{q}+\mathbf{p}-\mathbf{p}']}^{(1)} + \operatorname{sgn}(\gamma_{\mathbf{G}})M_{\mathbf{q},\mathbf{p},\mathbf{p}',[\mathbf{q}+\mathbf{p}-\mathbf{p}']}^{(2)}, \tag{4.10}$$

$$N_{\mathbf{q},\mathbf{p},\mathbf{p}'[\mathbf{q}+\mathbf{p}-\mathbf{p}']}^{(2)} = M_{\mathbf{q},\mathbf{p},\mathbf{p}',[\mathbf{q}+\mathbf{p}-\mathbf{p}']}^{(1)} + \operatorname{sgn}(\gamma_{\mathbf{G}})M_{\mathbf{q},\mathbf{p},\mathbf{p}',[\mathbf{q}+\mathbf{p}-\mathbf{p}']}^{(2)}.$$
(4.11)

Here $[\mathbf{q} + \mathbf{p} - \mathbf{p}']$ stands for $\mathbf{q} + \mathbf{p} - \mathbf{p}'$ reduced to the first MBZ by a reciprocal vector \mathbf{G} , that is, $[\mathbf{q} + \mathbf{p} - \mathbf{p}'] = \mathbf{q} + \mathbf{p} - \mathbf{p}' - \mathbf{G}$. Equation (4.8) and the first term of Eq. (4.9) arise from the spin-reduction factor with the diagram (a). The second and the third terms of Eq. (4.9) arise from the diagram (b), and the fourth term arises from the diagram (c). No contribution comes out from the diagram (d). A systematic study of the 1/S expansion for the dynamical structure factor has been carried out in Ref. 45.

Figure 5 shows the one-magnon intensity $y_1(\omega_i; \mathbf{q})$

within the LSW contribution, as a function of \mathbf{q} along symmetry lines, where ω_i is set to give rise to the peak in the absorption spectra. Since it is proportional to the dynamical structure factor, its \mathbf{q} -dependence is well known. The one-magnon intensity vanishes with $\mathbf{q} \to 0$, while diverges with $\mathbf{q} \to (\pi, \pi)$. The difference from the result of the UCL approximation is only its magnitude; the difference becomes larger with decreasing values of Γ .

Figure 6 shows the one-magnon intensity evaluated up to the first and the second order of 1/S [Eqs. (4.8) and

(4.9)]. The intensities are found strongly reduced from the zeroth-order values. The 1/S expansion has already been carried out to the transverse component of the dynamical structure factor (see Fig. 5 in Ref. 45).

Now we discuss the continuum spectra of three-magnon excitations. Analyzing carefully the diagrams in Fig. 4, we finally obtain from the second-order contribution with respect to 1/S as

$$y_{3}(\omega_{i}; \mathbf{q}, \omega) = N(2S)|f_{1}^{(1)}(\omega_{i})m_{\mathbf{q}} + f_{2}^{(1)}(\omega_{i})\ell_{\mathbf{q}}|^{2} \frac{1}{(2S)^{2}} \left(\frac{2}{N}\right)^{2} \sum_{\mathbf{p}, \mathbf{p}'} 2\pi\delta(\omega - \epsilon_{\mathbf{p}} - \epsilon_{\mathbf{p}'} - \epsilon_{\mathbf{q}+\mathbf{p}-\mathbf{p}'})$$

$$\times \frac{1}{2} \ell_{\mathbf{q}}^{2} \ell_{\mathbf{p}}^{2} \ell_{\mathbf{p}'}^{2} \ell_{\mathbf{q}+\mathbf{p}-\mathbf{p}'}^{2} \left| M_{\mathbf{q}, \mathbf{p}, \mathbf{p}', [\mathbf{q}+\mathbf{p}-\mathbf{p}']}^{(1)} + \operatorname{sgn}(\gamma_{\mathbf{G}}) M_{\mathbf{q}, \mathbf{p}, \mathbf{p}', [\mathbf{q}+\mathbf{p}-\mathbf{p}']}^{(2)} \right|$$

$$- 2 \left\{ \frac{B_{\mathbf{q}, \mathbf{p}, \mathbf{p}', [\mathbf{q}+\mathbf{p}-\mathbf{p}']}^{(4)}}{\epsilon_{\mathbf{q}} - \epsilon_{\mathbf{p}} - \epsilon_{\mathbf{p}'} - \epsilon_{\mathbf{q}+\mathbf{p}-\mathbf{p}']}} + \frac{\operatorname{sgn}(\gamma_{\mathbf{G}}) B_{\mathbf{q}, \mathbf{p}, \mathbf{p}', [\mathbf{q}+\mathbf{p}-\mathbf{p}']}^{(6)}}{\epsilon_{\mathbf{q}} + \epsilon_{\mathbf{p}} - \epsilon_{\mathbf{p}'} - \epsilon_{\mathbf{q}+\mathbf{p}-\mathbf{p}'}} \right\}^{2}.$$

$$(4.12)$$

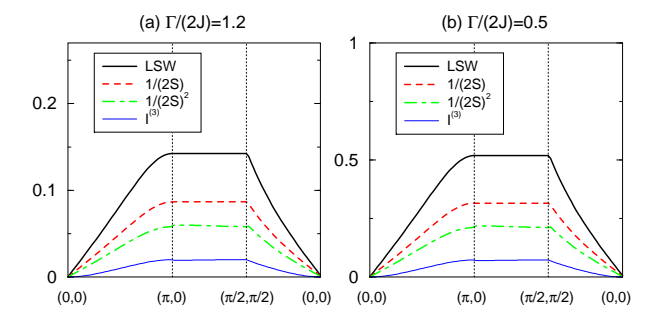


FIG. 6: (Color online) One-magnon intensity $y_1(\omega_i; \mathbf{q})/[N(2S)]$ up to the first (red broken line) and the second (green dot-dashed line) order of 1/S, as a function of \mathbf{q} along symmetry lines. The ω_i is set to give rise to the peak in the absorption spectra. The integrated intensity of three-magnon continuum $I^{(3)}(\omega_i; \mathbf{q})$ is also shown by blue thin line.

Note that Eq. (4.12) is, except for the prefactor, equal to Eq. (6.19) in Ref. 45, as it should be. The total intensity of three-magnon excitations is given by

$$I^{(3)}(\omega_i; \mathbf{q}) = \int_0^\infty y_3(\omega_i; \mathbf{q}, \omega) \frac{\mathrm{d}\omega}{2\pi}.$$
 (4.13)

Figures 6 (a) and (b) show calculated $I^{(3)}(\omega_i; \mathbf{q})$ along

symmetry lines for \mathbf{q} with ω_i corresponding to the peak in the absorption spectra. It is found that its intensity is about 20%-30% of the one-magnon intensity.

The magnon energy $\epsilon_{\bf q}$ is corrected as $\tilde{\epsilon}_{\bf q}=(1+A/2S)\epsilon_{\bf q}$ within the first-order in 1/S. The second-order correction in 1/S, which is known to be rather small (see Ref. 30 for the details). We replace $\delta(\omega-\epsilon_{\bf q})$ by $\delta(\omega-\tilde{\epsilon}_{\bf q})$ in Eq. (4.6) and $\delta(\omega-\epsilon_{\bf p}-\epsilon_{\bf p'}-\epsilon_{q+p-p'})$ by $\delta(\omega-\tilde{\epsilon}_{\bf p}-\tilde{\epsilon}_{\bf p'}-\tilde{\epsilon}_{q+p-p'})$ in Eq. (4.12), respectively. Figure 7 shows the spin-flip correlation function $Y^{(1)}(\omega_i;{\bf q},\omega)/N(2S)$ as a function of ω along symmetry lines for ${\bf q}$. The spectra consist of the δ -function peak shown by vertical lines and the continuum of three-magnon excitations.

B. Spin-conserving excitation spectra

The two-magnon operator $Z^{(2)}(\omega_i; \mathbf{q})$ defined by Eq. (3.33) is rewritten in terms of magnon operators by using Eqs. (A1)-(A10). The result is summarized as

$$Z^{(2)}(\omega_i; \mathbf{q}) = (2S) \sum_{\mathbf{k}} N(\omega_i; \mathbf{q}, \mathbf{k}) \alpha_{[\mathbf{q} + \mathbf{k}]}^{\dagger} \beta_{-\mathbf{k}}^{\dagger} + \cdots,$$
(4.14)

with

$$N(\omega_{i}; \mathbf{q}, \mathbf{k}) = f_{2}^{(2)}(\omega_{i}) \Big\{ (1 + \gamma_{\mathbf{q}})(\ell_{[\mathbf{q}+\mathbf{k}]} m_{\mathbf{k}} + \operatorname{sgn}(\gamma_{\mathbf{G}}) \ell_{\mathbf{k}} m_{[\mathbf{q}+\mathbf{k}]}) + \ell_{[\mathbf{q}+\mathbf{k}]} \ell_{\mathbf{k}}(\gamma_{\mathbf{k}} + \operatorname{sgn}(\gamma_{\mathbf{G}}) \gamma_{[\mathbf{q}+\mathbf{k}]}) + m_{[\mathbf{q}+\mathbf{k}]} m_{\mathbf{k}}(\gamma_{[\mathbf{q}+\mathbf{k}]} + \operatorname{sgn}(\gamma_{\mathbf{G}}) \gamma_{\mathbf{k}}) \Big\},$$

$$(4.15)$$

where $[\mathbf{q} + \mathbf{k}]$ stands for the $\mathbf{q} + \mathbf{k}$ reduced in the first MBZ by a reciprocal lattice vector \mathbf{G} , that is, $[\mathbf{q} + \mathbf{k}] =$

 $\mathbf{q} + \mathbf{k} - \mathbf{G}$. In deriving Eq. (4.14), the non-linear terms

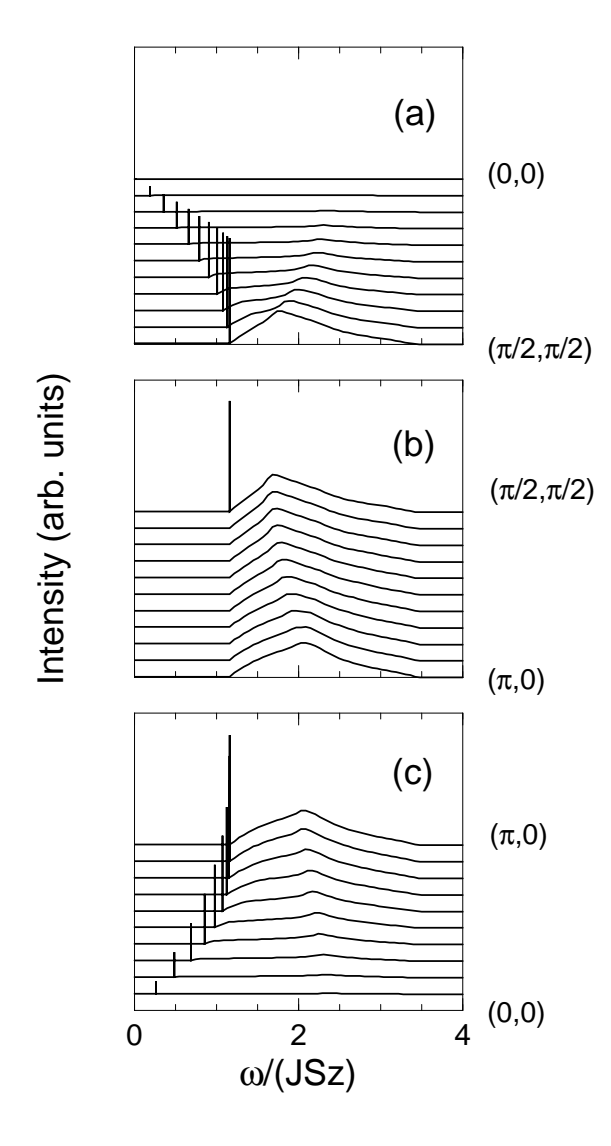


FIG. 7: Spin-flip correlation function $Y^{(1)}(\omega_i; \mathbf{q}, \omega)/[N(2S)]$ as a function of energy loss ω along symmetry lines for \mathbf{q} . Vertical solid lines represent the δ -function peak of the one-magnon excitation. On panel (b), only one vertical line is shown, since the peak positions and the weights of the one-magnon excitations are nearly the same for $(\pi, 0) - (\pi/2, \pi/2)$.

in the expansion of S^{\pm} with magnon operators have been neglected, since the consistent analysis within the 1/S expansion is quite complicated. Such terms may cause the intensity transfer to the four-magnon excitations. This type of correlation function has been studied for the magnetic excitations in the K-edge RIXS. 11,25

Since two-magnons are excited closely to each other around the core-hole site, the magnon-magnon interaction would be important. Introducing the two-magnon Green function,

$$F(\mathbf{q}, \omega; \mathbf{k}, \mathbf{k}') = -i \int e^{i\omega t} dt \langle T[\beta_{-\mathbf{k}}(t)\alpha_{[\mathbf{q}+\mathbf{k}]}(t)\alpha_{[\mathbf{q}+\mathbf{k}']}^{\dagger}\beta_{-\mathbf{k}'}^{\dagger}] \rangle,$$
(4.16)

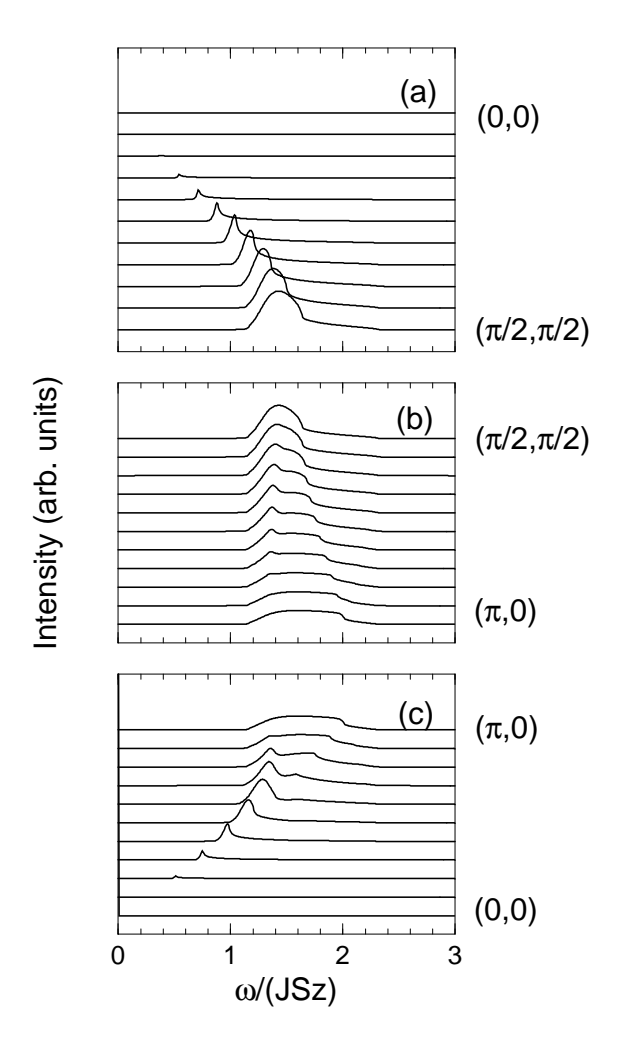


FIG. 8: Spin-conserving correlation function $Y^{(2)}(\omega_i; \mathbf{q}, \omega)/[N(2S)^2]$ as a function of energy loss ω along symmetry lines for \mathbf{q} .

we take account of scattering of two magnons through the term $B_{1234}^{(3)}$ [Eq. (A16)]. Applying the addition theorem of trigonometric functions to factors such as γ_{2-4} in $B_{1234}^{(3)}$, we could transform $B_{1234}^{(3)}$ into a separable form. Thereby we obtain the t-matrix by summing up the ladder diagrams in a closed form. We have already explained this procedure in the analysis of the two-magnon spectra in the K-edge RIXS. See Ref. 25 for the details. Once we obtain the Green function, by the fluctuation-dissipation theorem, we obtain the correlation function as

$$Y^{(2)}(\omega_i; \mathbf{q}, \omega) = (2S)^2 \sum_{\mathbf{k}} \sum_{\mathbf{k'}} N^*(\omega_i; \mathbf{q}, \mathbf{k}) N(\omega_i; \mathbf{q}, \mathbf{k'})$$

$$\times (-2) \operatorname{Im} F(\mathbf{q}, \omega; \mathbf{k}, \mathbf{k'}). \tag{4.17}$$

Figure 8 shows $Y^{(2)}(\omega_i; \mathbf{q}, \omega)$ as a function of ω along symmetry lines for \mathbf{q} with ω_i corresponding to the peak in the absorption spectra.

The frequency-integrated correlation function is not changed by the presence of the magnon-magnon interaction. Neglecting the interaction in the calculation of

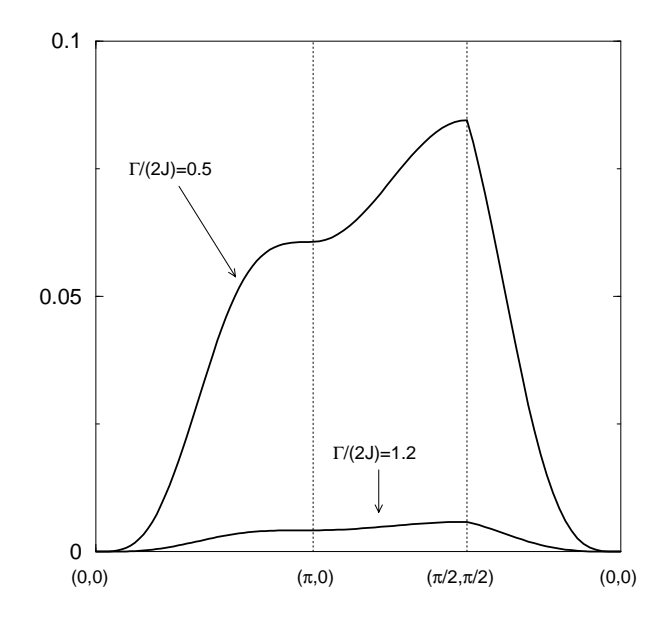


FIG. 9: Frequency-integrated correlation function $Y^{(2)}(\omega_i; \mathbf{q})/[N(2S)^2]$ as a function of \mathbf{q} along symmetry lines. The ω_i is set to give rise to the peak in the absorption spectra.

 $F(\mathbf{q}, \omega; \mathbf{k}, \mathbf{k}')$ in Eq. (4.17), we simply obtain

$$Y^{(2)}(\omega_i; \mathbf{q}) \equiv \int Y^{(2)}(\omega_i : \mathbf{q}, \omega) \frac{\mathrm{d}\omega}{2\pi}$$
$$= (2S)^2 \sum_{\mathbf{k}} |N(\omega_i; \mathbf{q}, \mathbf{k})|^2. \quad (4.18)$$

Figure 9 shows $Y^{(2)}(\omega_i; \mathbf{q})/N(2S)^2$ as a function of \mathbf{q} along symmetry lines with ω_i corresponding to the peak in the absorption spectra. The values are about one order of magnitude smaller than those of $Y^{(1)}(\omega_i; \mathbf{q})/[N(2S)]$.

V. SPECTRAL SHAPE IN COMPARISON WITH EXPERIMENTS

In this section, we analyze specifically the Cu L_3 edge spectra in $\mathrm{Sr_2CuO_2Cl_2}$. According to the experimental setup shown in Fig. 1(a) of Ref. 35, the photon comes onto the a-b (x-y) plane, and is scattered with the angle 130 degrees to the incident direction. The a-c (x-z) plane is set as the scattering plane. The polarization vector of the incident photon is then expressed as $\boldsymbol{\alpha}_i = (0, -1, 0)$ for the σ polarization and $\boldsymbol{\alpha}_i = (\chi_i^{\pi}, 0, \zeta_i^{\pi})$ for the π polarization. Similarly, the polarization of the scattered photon is expressed as $\boldsymbol{\alpha}_f = (0, -1, 0)$ for the σ' polarization and $\boldsymbol{\alpha}_f = (\chi_f^{\pi}, 0, \zeta_f^{\pi})$ for the π' polarization. Thereby we have from Table II,

$$P^{(1)}(3/2, \alpha^f, \alpha^i) = 0, \quad P^{(0)}(3/2, \alpha^f, \alpha^i) = \frac{2}{15}, \quad (\sigma \to \sigma'),$$
 (5.1)

$$P^{(1)}(3/2, \alpha^f, \alpha^i) = -\frac{i}{15} \chi_f^{\pi}, \quad P^{(0)}(3/2, \alpha^f, \alpha^i) = 0, \quad (\sigma \to \pi'), \tag{5.2}$$

$$P^{(1)}(3/2, \alpha^f, \alpha^i) = 0, \quad P^{(0)}(3/2, \alpha^f, \alpha^i) = \frac{2}{15} \chi_f^{\pi} \chi_i^{\pi}, \quad (\pi \to \pi'), \tag{5.3}$$

$$P^{(1)}(3/2, \alpha^f, \alpha^i) = \frac{i}{15} \chi_i^{\pi}, \quad P^{(0)}(3/2, \alpha^f, \alpha^i) = 0, \quad (\pi \to \sigma').$$
 (5.4)

The polarization is separated with the incident photon, but not separated with the scattered photon in the experiment. In this situation, the RIXS spectra, which depend on the polarization of the incident photon, are expressed from Eqs. (5.1)-(5.4) as

$$I(\omega_i; \mathbf{q}, \omega) = \frac{w^4}{4\omega_i \omega_f} \times \left\{ \begin{bmatrix} \left(\frac{\chi_f^{\pi}}{15}\right)^2 Y^{(1)}(\omega_i; \mathbf{q}, \omega) + \left(\frac{2}{15}\right)^2 Y^{(2)}(\omega_i; \mathbf{q}, \omega) \end{bmatrix}, \quad (\sigma - \text{pol.}), \\ \left(\frac{\chi_i^{\pi}}{15}\right)^2 Y^{(1)}(\omega_i; \mathbf{q}, \omega) + \left(\frac{2}{15}\right)^2 \left(\chi_f^{\pi} \chi_i^{\pi}\right)^2 Y^{(2)}(\omega_i; \mathbf{q}, \omega) \right], \quad (\pi - \text{pol.}), \end{cases}$$
(5.5)

where **q** is regarded as the component (of the transferred momentum) projected onto the a-b plane. For the spin-flip excitations, the intensity in the π polarization is larger (or smaller) by a factor $(\chi_i^{\pi}/\chi_f^{\pi})^2$ than that in

the σ polarization. For the spin-conserving excitations, the intensity in the π polarization is smaller by a factor $(\chi_f^{\pi}\chi_i^{\pi})^2$ than that in the σ polarization. Notice that, in both cases, the intensity ratio between in the π polariza-

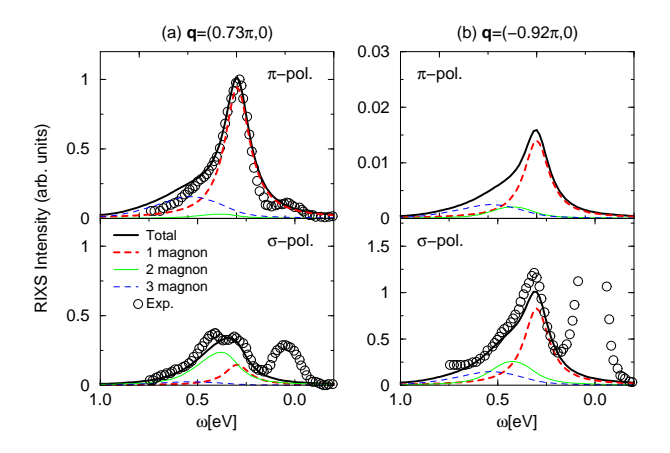


FIG. 10: (Color online) RIXS spectra as a function of energy loss ω for the momentum transfer projected onto the a-b plane: panel (a) for $\mathbf{q}=(0.73\pi,0)$, and panel (b) for $\mathbf{q}=(-0.92\pi,0)$. The incident photon energy ω_i is set to give rise to the peak in the absorption spectra. J=130 meV, and the calculated spectra are convoluted with the Lorentzian function with the half width of half maximum 78 meV. The experimental data for $\mathrm{Sr_2CuO_2Cl_2}$ are taken from Ref. 35; the peak height is adjusted to coincide with the calculated one in the π polarization for $\mathbf{q}=(0.73\pi,0)$, while it is adjusted with the calculated one in the σ polarization for $\mathbf{q}=(-0.92\pi,0)$. The thick solid (black) lines represent the total intensities. The thick dotted (red), thin solid (green) and thin dotted (blue) lines correspond to the one, two, and three magnon contributions, respectively.

tion and in the σ polarization is completely determined from the scattering geometry. That is, the ratio is independent of the values of the correlation functions.

Figure 10 shows the calculated result with ω_i giving rise to the peak in the absorption spectra. For comparison with the experiment,³⁵ the exchange coupling constant J is assumed to be 130 meV, which is nearly the same as the one estimated by the inelastic neutron scattering experiment in La₂CuO₄.⁴⁷ The calculated spectra are convoluted with the Lorentzian function with the half width of half maximum 78 meV in accordance with the experimental resolution. Panel (a) shows the spectra for $\mathbf{q} = (0.73\pi, 0)$. According to the experimental setup, we have $\chi_i^{\pi} = -0.95$ and $\chi_f^{\pi} = 0.38$. The experimental data are drawn such that the peak height coincides with the calculated peak in the π polarization. In the π polarization, the spin-conserving contribution is suppressed by the relative weight $(2\chi_f^{\pi})^2 = 0.58$, and the spectra are dominated by the spin-flip contribution. The spin-flip contribution includes the three-magnon continuum with the energy higher than the single-magnon peak. This makes the spectral shape asymmetric in agreement with the experimental data in the π polarization. In the σ polarization, the spin-flip contribution becomes smaller by a factor $(\chi_f^{\pi}/\chi_i^{\pi})^2 = 0.16$ than that in the π polarization, while the spin-conserving contribution becomes larger by a factor $1/(\chi_f^{\pi}\chi_i^{\pi})^2 = 7.7$ than that in the π polarization, and thereby the two-magnon intensity becomes larger in

comparison with the one-magnon intensity. In the experiment, the spectra consist of two peaks; 35 the low-energy peak is considered to come from the one-magnon excitation, which intensity is estimated to be smaller by a factor 0.32 than the one-magnon intensity in the π polarization. This value is about twice the theoretical value, and the reason for this discrepancy is not known, since the value is determined by the geometry. In the calculated spectra, the one-magnon and two-magnon peaks are closely located, forming a single peak. However, the spectral shape is asymmetric with a broad width in agreement with the experiment, and the total intensity is also in good agreement with the experiment.

Panel (b) shows the spectra for $\mathbf{q} = (-0.92\pi, 0)$. According to the experimental setup, we have $\chi_i^{\pi} = -0.11$, $\chi_f^{\pi} = 0.85$. Since $(\chi_i^{\pi}/\chi_f^{\pi})^2 = 0.016$ and $(\chi_i^{\pi}\chi_f^{\pi})^2 = 0.0087$, the intensity in the π polarization is two order of magnitude smaller than that in the σ polarization. In the σ polarization, the two-magnon intensity has a considerable weight, resulting in a shoulder in the high energy side. The overall shape with a considerable width agrees well with the experiment.

VI. CONCLUDING REMARKS

We have studied the magnetic excitations in the L-edge RIXS in undoped cuprates. We have analyzed in detail the second-order dipole allowed process with paying attention to the strong perturbation through the intermediate state, in which there is no spin degree of freedom at the core-hole site. In this situation, it is not logically appropriate to make a perturbation calculation with the terms involving the spin degree of freedom lost in the intermediate state. Within the approximation that the perturbation due to the intermediate state is not extending to neighboring sites, we derive the spin-flip final state expressed as $\alpha_{f\perp} \times \alpha_{i\perp} \cdot \mathbf{S}_0 |g\rangle$ in the scattering channel with changing the polarization, which leads to the RIXS spectra expressed as the dynamical structure factor of the transverse spin component. In the scattering channel without changing the polarization, we have assumed a spherical form of the spin-conserving final state, $\mathbf{X} \cdot \mathbf{S}_0 | g \rangle$, which leads to the RIXS spectra expressed as the 'exchange'-type multi-spin correlation function. We have numerically evaluated the transition amplitudes for both the spin-flip and the spin-conserving final states on a finite-size cluster centered at the core-hole site.

Since no core hole exists in the final state, the spin excitations could move around the crystal. We have treated the itinerant spin excitations by means of the 1/S-expansion method, which is known to work for treating the quantum fluctuation in the two-dimensional Heisenberg antiferromagnet. For the spin-flip excitations, having expanded the spin-flip operators up to the second order of 1/S, we have obtained the three-magnon excitations in addition to the one-magnon excitations. This gives rise to a considerable reduction of the one-

magnon intensity as well as the intensity transfer to the three-magnon continuum. For the spin-conserving excitations, we have taken into account the interaction between magnons by summing up the ladder diagrams.

We have analyzed the Cu L_3 -edge spectra in $Sr_2CuO_2Cl_2$ on the basis of these results. The two- and three-magnon excitations give rise to substantial intensities in the high energy side of the one-magnon peak as a function of energy loss, in good agreement with the experiment.³⁵ We hope that the similar analyses are applied to the RIXS spectra in other materials and clarify the nature of magnetic excitations in future.

Acknowledgments

The authors thank to Prof. J. van den Brink for useful discussion. This work was partially supported by a Grant-in-Aid for Scientific Research from the Ministry of Education, Culture, Sports, Science and Technology of the Japanese Government.

Appendix A: 1/S expansion

We summarize briefly the 1/S expansion method in the Heisenberg antiferromagnet. For details, see Refs. 30 and 45. The x, y, z axes below are interpreted as the x', y', z' axes in the text.

a. Hamiltonian

Assuming two sublattices in the antiferromagnetic ground state, we express spin operators by boson operators as

$$S_i^z = S - a_i^{\dagger} a_i, \tag{A1}$$

$$S_i^+ = (S_i^-)^\dagger = \sqrt{2S} f_i(S) a_i,$$
 (A2)

$$S_i^z = -S + b_i^{\dagger} b_j, \tag{A3}$$

$$S_{j}^{+} = (S_{j}^{-})^{\dagger} = \sqrt{2S}b_{j}^{\dagger}f_{j}(S),$$
 (A4)

where a_i and b_j are boson annihilation operators, and

$$f_{\ell}(S) = \left(1 - \frac{n_{\ell}}{2S}\right)^{1/2} = 1 - \frac{1}{2} \frac{n_{\ell}}{2S} - \frac{1}{8} \left(\frac{n_{\ell}}{2S}\right)^{2} + \cdots, (A5)$$

with $n_{\ell} = a_i^{\dagger} a_i$ and $b_j^{\dagger} b_j$. Indices i and j refer to sites on the up and down sublattices, respectively. Using Eqs. (A1)-(A4), H_{mag} may be expanded in powers of 1/S,

$$H_{\text{mag}} = -\frac{1}{2}JS^2Nz + H_{\text{mag}}^{(0)} + H_{\text{mag}}^{(1)} + H_{\text{mag}}^{(2)} + \cdots, (A6)$$

where N and z are the number of lattice sites and that of nearest neighbor sites, respectively. The leading term $H_{\text{mag}}^{(0)}$ is expressed as

$$H_{\text{mag}}^{(0)} = JS \sum_{\langle i,j \rangle} (a_i^{\dagger} a_i + b_j^{\dagger} b_j + a_i b_j + a_i^{\dagger} b_j^{\dagger}).$$
 (A7)

The Fourier transforms of the boson operators are introduced within the first magnetic Brillouin zone (MBZ),

$$a_i = \left(\frac{2}{N}\right)^{1/2} \sum_{\mathbf{k}} a_{\mathbf{k}} \exp(i\mathbf{k} \cdot \mathbf{r}_i),$$
 (A8)

$$b_j = \left(\frac{2}{N}\right)^{1/2} \sum_{\mathbf{k}} b_{\mathbf{k}} \exp(i\mathbf{k} \cdot \mathbf{r}_j). \tag{A9}$$

Then, we introduce a Bogoliubov transformation,

$$a_{\mathbf{k}}^{\dagger} = \ell_{\mathbf{k}} \alpha_{\mathbf{k}}^{\dagger} + m_{\mathbf{k}} \beta_{-\mathbf{k}}, \quad b_{-\mathbf{k}} = m_{\mathbf{k}} \alpha_{\mathbf{k}}^{\dagger} + \ell_{\mathbf{k}} \beta_{-\mathbf{k}}, \quad (A10)$$

with

$$\ell_{\mathbf{k}} = \left[\frac{1+\epsilon_{\mathbf{k}}}{2\epsilon_{\mathbf{k}}}\right]^{1/2}, \quad m_{\mathbf{k}} = -\left[\frac{1-\epsilon_{\mathbf{k}}}{2\epsilon_{\mathbf{k}}}\right]^{1/2} \equiv -x_{\mathbf{k}} \ell_{\mathbf{k}} 11$$

$$\epsilon_{\mathbf{k}} = \sqrt{1-\gamma_{\mathbf{k}}^{2}}, \quad \gamma_{\mathbf{k}} = \frac{1}{z} \sum_{\boldsymbol{\delta}} e^{i\mathbf{k}\cdot\boldsymbol{\delta}}, \quad (A12)$$

where δ connects the origin with the nearest neighbor sites. By this transformation, $H_{\rm mag}^{(0)}$ is diagonalized as

$$H_{\text{mag}}^{(0)} = JSz \sum_{\mathbf{k}} (\epsilon_{\mathbf{k}} - 1) + JSz \sum_{\mathbf{k}} \epsilon_{\mathbf{k}} (\alpha_{\mathbf{k}}^{\dagger} \alpha_{\mathbf{k}} + \beta_{\mathbf{k}}^{\dagger} \beta_{\mathbf{k}}).$$
(A13)

Similarly, $H_{\text{mag}}^{(1)}$ is expressed as

$$H_{\text{mag}}^{(1)} = \frac{JSz}{2S} A \sum_{\mathbf{k}} \epsilon_{\mathbf{k}} (\alpha_{\mathbf{k}}^{\dagger} \alpha_{\mathbf{k}} + \beta_{\mathbf{k}}^{\dagger} \beta_{\mathbf{k}})$$

$$+ \frac{-JSz}{2SN} \sum_{1234} \delta_{\mathbf{G}} (1 + 2 - 3 - 4) \ell_{1} \ell_{2} \ell_{3} \ell_{4}$$

$$\times \left[\alpha_{1}^{\dagger} \alpha_{2}^{\dagger} \alpha_{3} \alpha_{4} B_{1234}^{(1)} + \beta_{-3}^{\dagger} \beta_{-4}^{\dagger} \beta_{-1} \beta_{-2} B_{1234}^{(2)} + 4 \alpha_{1}^{\dagger} \beta_{-4}^{\dagger} \beta_{-2} \alpha_{3} B_{1234}^{(3)} + (2 \alpha_{1}^{\dagger} \beta_{-2} \alpha_{3} \alpha_{4} B_{1234}^{(4)} + 2 \beta_{-4}^{\dagger} \beta_{-1} \beta_{-2} \alpha_{3} B_{1234}^{(5)} + \alpha_{1}^{\dagger} \alpha_{2}^{\dagger} \beta_{-3}^{\dagger} \beta_{-4}^{\dagger} B_{1234}^{(6)} + \text{H.c.} \right]. \tag{A14}$$

Here the first term in Eq. (A14) is known as the Oguchi correction, 26 which coefficient A is given by

$$A = \frac{2}{N} \sum_{\mathbf{k}} (1 - \epsilon_{\mathbf{k}}). \tag{A15}$$

For the square lattice, A=0.1579. The second term represents the interaction between magnons, where \mathbf{k}_1 , \mathbf{k}_2 , \mathbf{k}_3 , \cdots are abbreviated as $1,2,3,\cdots$, and the Kronecker delta $\delta_{\mathbf{G}}(1+2-3-4)$ indicates the conservation of momenta within a reciprocal lattice vector \mathbf{G} . The vertex functions $B^{(i)}$'s in a symmetric parametrization are given in Ref. 27 and 30. For example, $B_{1234}^{(3)}$, which describes the scattering of two magnons, is given by

$$B_{1234}^{(3)} = \gamma_{2-4} + \gamma_{1-3}x_1x_2x_3x_4 + \gamma_{1-4}x_1x_2 + \gamma_{2-3}x_3x_4 - \frac{1}{2}(\gamma_2x_4 + \gamma_1x_1x_2x_4 + \gamma_{2-3-4}x_3 + \gamma_{1-3-4}x_1x_2x_3 + \gamma_4x_2 + \gamma_3x_2x_3x_4 + \gamma_{4-2-1}x_1 + \gamma_{3-2-1}x_1x_3x_4).$$
(A16)

The second-order term $H_{\text{mag}}^{(2)}$ is composed of products of six boson operators. Writing it in a normal product form with respect to spin-wave operators, we have

$$H_{\text{mag}}^{(2)} = \frac{JSz}{(2S)^2} \sum_{\mathbf{k}} \left[C_1(\mathbf{k}) (\alpha_{\mathbf{k}}^{\dagger} \alpha_{\mathbf{k}} + \beta_{\mathbf{k}}^{\dagger} \beta_{\mathbf{k}}) + C_2(\mathbf{k}) (\alpha_{\mathbf{k}}^{\dagger} \beta_{-\mathbf{k}}^{\dagger} + \beta_{-\mathbf{k}} \alpha_{\mathbf{k}}) + \cdots \right].$$
(A17)

Neglected terms are unnecessary for calculating corrections up to the second order. The explicit forms of $C_1(\mathbf{k})$ and $C_2(\mathbf{k})$, are given by Eqs. (2.22) and (2.23) in Ref. 30.

b. the Green function

We introduce the Green functions for spin-waves,

$$G_{\alpha\alpha}(\mathbf{k},t) = -i\langle T(\alpha_{\mathbf{k}}(t)\alpha_{\mathbf{k}}^{\dagger}(0))\rangle, \tag{A18}$$

$$G_{\alpha\beta}(\mathbf{k},t) = -i\langle T(\alpha_{\mathbf{k}}(t)\beta_{-\mathbf{k}}(0))\rangle,$$
 (A19)

$$G_{\beta\alpha}(\mathbf{k},t) = -i\langle T(\beta_{-\mathbf{k}}^{\dagger}(t)\alpha_{\mathbf{k}}^{\dagger}(0))\rangle,$$
 (A20)

$$G_{\beta\beta}(\mathbf{k},t) = -i\langle T(\beta_{-\mathbf{k}}^{\dagger}(t)\beta_{-\mathbf{k}}(0))\rangle,$$
 (A21)

where $\langle \cdots \rangle$ denotes the expectation value over the ground state, and T is the time-ordering operator. Measuring energies in units of JSz, the unperturbed propagators corresponding to $H_{\rm mag}^{(0)}$ are given by

$$G_{\alpha\alpha}^{0}(\mathbf{k},\omega) = [\omega - \epsilon_{\mathbf{k}} + i\delta]^{-1},$$
 (A22)

$$G_{\alpha\beta}^{0}(\mathbf{k},\omega) = G_{\beta\alpha}^{0}(\mathbf{k},\omega) = 0,$$
 (A23)

$$G_{\beta\beta}^{0}(\mathbf{k},\omega) = [-\omega - \epsilon_{\mathbf{k}} + i\delta]^{-1}.$$
 (A24)

The self-energy is defined by a matrix Dyson's equation 27

$$G_{\mu\nu}(\mathbf{k},\omega) = G^{0}_{\mu\nu}(\mathbf{k},\omega)$$

$$+ \sum_{\mu'\nu'} G^{0}_{\mu\mu'}(\mathbf{k},\omega) \Sigma_{\mu'\nu'}(\mathbf{k},\omega) G_{\nu'\nu}(\mathbf{k},\omega).$$
(A25)

It is expanded in powers of 1/(2S),

$$\Sigma_{\mu\nu}(\mathbf{k},\omega) = \frac{1}{2S} \Sigma_{\mu\nu}^{(1)}(\mathbf{k},\omega) + \frac{1}{(2S)^2} \Sigma_{\mu\nu}^{(2)}(\mathbf{k},\omega) + \cdots$$
(A26)

The first-order terms are obtained from H_1 :

$$\Sigma_{\alpha\alpha}^{(1)}(\mathbf{k},\omega) = \Sigma_{\beta\beta}^{(1)}(\mathbf{k},\omega) = A\epsilon_{\mathbf{k}},$$

$$\Sigma_{\alpha\beta}^{(1)}(\mathbf{k},\omega) = \Sigma_{\beta\alpha}^{(1)}(\mathbf{k},\omega) = 0.$$
(A27)

The second-order term $\Sigma_{\mu\nu}^{(2)}(\mathbf{k},\omega)$ is given by the second-order perturbation:

$$\Sigma_{\alpha\alpha}^{(2)}(\mathbf{k},\omega) = C_{1}(\mathbf{k}) + \left(\frac{2}{N}\right)^{2} \sum_{\mathbf{pq}} 2\ell_{\mathbf{k}}^{2} \ell_{\mathbf{p}}^{2} \ell_{\mathbf{q}}^{2} \ell_{\mathbf{k}+\mathbf{p}-\mathbf{q}}^{2} \left[\frac{|B_{\mathbf{k},\mathbf{p},\mathbf{q},[\mathbf{k}+\mathbf{p}-\mathbf{q}]}^{(4)}|^{2}}{\omega - \epsilon_{\mathbf{p}} - \epsilon_{\mathbf{q}} - \epsilon_{\mathbf{k}+\mathbf{p}-\mathbf{q}} + i\delta} - \frac{|B_{\mathbf{k},\mathbf{p},\mathbf{q},[\mathbf{k}+\mathbf{p}-\mathbf{q}]}^{(6)}|^{2}}{\omega + \epsilon_{\mathbf{p}} + \epsilon_{\mathbf{q}} + \epsilon_{\mathbf{k}+\mathbf{p}-\mathbf{q}} - i\delta} \right]$$

$$= \Sigma_{\beta\beta}^{(2)}(-\mathbf{k}, -\omega), \qquad (A28)$$

$$\Sigma_{\alpha\beta}^{(2)}(\mathbf{k},\omega) = C_{2}(\mathbf{k}) + \left(\frac{2}{N}\right)^{2} \sum_{\mathbf{pq}} 2\ell_{\mathbf{k}}^{2} \ell_{\mathbf{p}}^{2} \ell_{\mathbf{q}}^{2} \ell_{\mathbf{k}+\mathbf{p}-\mathbf{q}}^{2} \operatorname{sgn}(\gamma_{\mathbf{G}}) B_{\mathbf{k},\mathbf{p},\mathbf{q},[\mathbf{k}+\mathbf{p}-\mathbf{q}]}^{(4)} B_{\mathbf{k},\mathbf{p},\mathbf{q},[\mathbf{k}+\mathbf{p}-\mathbf{q}]}^{(6)} \frac{2(\epsilon_{\mathbf{p}} + \epsilon_{\mathbf{q}} + \epsilon_{\mathbf{k}+\mathbf{p}-\mathbf{q}})}{\omega^{2} - (\epsilon_{\mathbf{p}} + \epsilon_{\mathbf{q}} + \epsilon_{\mathbf{k}+\mathbf{p}-\mathbf{q}})^{2} + i\delta}$$

$$= \Sigma_{\beta\alpha}^{(2)}(-\mathbf{k}, -\omega), \qquad (A29)$$

where $\delta \to 0$, and $[\mathbf{k} + \mathbf{p} - \mathbf{q}]$ stands for $\mathbf{k} + \mathbf{p} - \mathbf{q}$ reduced to the 1st MBZ by a reciprocal vector \mathbf{G} , that is, $[\mathbf{k} + \mathbf{p} - \mathbf{p}'] = \mathbf{k} + \mathbf{p} - \mathbf{p}' - \mathbf{G}$. In deriving Eqs. (A28) and (A29), we have used the relations,

$$B_{[\mathbf{k}+\mathbf{p}-\mathbf{q}],\mathbf{q},\mathbf{p},\mathbf{k}}^{(5)} = \operatorname{sgn}(\gamma_{\mathbf{G}}) B_{\mathbf{k},\mathbf{p},\mathbf{q},[\mathbf{k}+\mathbf{p}-\mathbf{q}]}^{(4)},$$

$$B_{\mathbf{q},[\mathbf{k}+\mathbf{p}-\mathbf{q}],\mathbf{k},\mathbf{p}}^{(6)} = \operatorname{sgn}(\gamma_{\mathbf{G}}) B_{\mathbf{k},\mathbf{p},\mathbf{q},[\mathbf{k}+\mathbf{p}-\mathbf{q}]}^{(6)}.$$
(A30)

¹ C. -C. Kao, W. A. L. Caliebe, J. B. Hastings, and J. -M. Gillet, Phys. Rev. B **54**, 16361 (1996).

² J. P. Hill, C. -C. Kao, W. A. L. Caliebe, M. Matsubara, A. Kotani, J. L. Peng, and R. L. Greene, Phys. Rev. Lett. 80, 4967 (1998).

³ M. Z. Hasan, E. D. Isaacs, Z. -X. Shen, L. L. Miller, K. Tsutsui, T. Tohyama, and S. Maekawa, Science 288, 1811 (2000).

⁴ Y. J. Kim, J. P. Hill, C. A. Burns, S. Wakimoto, R. J. Birgeneau, D. Casa, T. Gog, and C. T. Venkataraman, Phys. Rev. Lett. 89, 177003 (2002).

⁵ T. Inami, T. Fukuda, J. Mizuki, S. Ishihara, H. Kondo, H. Nakao, T. Matsumura, K. Hirota, Y. Murakami, S. Maekawa, et al., Phys. Rev. B 67, 045108 (2003).

⁶ Y. J. Kim, J. P. Hill, H. Benthien, F. H. L. Essler, É. Jeckelmann, H. S. Choi, T. W. Noh, N. Motoyama, K. M. Kojima, S. Uchida, et al., Phys. Rev. Lett. **92**, 137402 (2004).

⁷ S. Suga, S. Imada, A. Higashiya, A. Shigemoto, S. Kasai, M. Sing, H. Fujiwara, A. Sekiyama, A. Yamasaki, C. Kim, et al., Phys. Rev. B **72**, 081101(R) (2005).

⁸ K. Tsutsui, T. Tohyama, and S. Maekawa, Phys. Rev. Lett. 83, 3705 (1999).

⁹ K. Okada and A. Kotani, J. Phys. Soc. Jpn. **75**, 044702 (2006).

J. van den Brink and M. van Veenendaal, Europhys. Lett. 73, 121 (2006).

¹¹ L. J. P. Ament, F. Forte, and J. van den Brink, Phys. Rev. B **75**, 115118 (2007).

¹² T. Nomura and J. Igarashi, J. Phys. Soc. Jpn. **73**, 1677 (2004).

¹³ T. Nomura and J. I. Igarashi, Phys. Rev. B **71**, 035110 (2005).

¹⁴ J. I. Igarashi, T. Nomura, and M. Takahashi, Phys. Rev. B **74**, 245122 (2006).

¹⁵ In the derivation, the Born approximation has been used to the core-hole potential, which is not weak. The approximation has partly been justified by examining higher-order corrections. See Ref. 14.

 $^{16}\,$ L. V. Keldysh, Sov. Phys. JETP ${\bf 20},\,1018$ (1965).

¹⁷ P. Nozières and E. Abrahams, Phys. Rev. B **10**, 3099 (1974).

¹⁸ M. Takahashi, J. I. Igarashi, and T. Nomura, Phys. Rev. B **75**, 235113 (2007).

¹⁹ T. Semba, M. Takahashi, and J. I. Igarashi, Phys. Rev. B 78, 155111 (2008).

²⁰ J. P. Hill, G. Blumberg, Y. -J. Kim, D. S. Ellis, S. Wakimoto, R. J. Birgeneau, S. Komiya, Y. Ando, B. Liang, R. L. Greene, et al., Phys. Rev. Lett. **100**, 097001 (2008).

²¹ D. S. Ellis, J. Kim, J. P. Hill, S. Wakimoto, R. J. Birgeneau, Y. Shvyd'ko, D. Casa, T. Gog, K. Ishii, K. Ikeuchi, et al., Phys. Rev. B 81, 085124 (2010).

²² J. van den Brink, cond-mat/0510140.

²³ J. van den Brink, Europhys. Lett. **80**, 47003 (2007).

²⁴ F. Forte, L. J. P. Ament, and J. van den Brink, Phys. Rev. B 77, 134428 (2008).

²⁵ T. Nagao and J. I. Igarashi, Phys. Rev. B **75**, 214414 (2007).

²⁶ T. Oguchi, Phys. Rev. **117**, 117 (1960).

A. B. Harris, D. Kumar, B. I. Halperin, and P. C. Hohenberg, Phys. Rev. B 3, 961 (1971).

²⁸ C. J. Hamer, Z. Weihong, and P. Arndt, Phys. Rev. B 46, 6276 (1992).

²⁹ C. M. Canali, S. M. Girvin, and M. Wallin, Phys. Rev. B 45, 10131 (1992).

³⁰ J. I. Igarashi, Phys. Rev. B **46**, 10763 (1992).

³¹ J. Igarashi, J. Phys.: Codens. Matter **4**, 10265 (1992).

³² G. Ghiringhelli, N. B. Brookes, E. Annese, H. Berger, C. Dallera, M. Grioni, L. Perfetti, A. Tagliaferri, and L. Braicovich, Phys. Rev. Lett. 92, 117406 (2004).

³³ L. Braicovich, L. J. P. Ament, V. Bisogni, F. Forte, C. Aruta, G. Balestrino, N. B. Brookes, G. M. De Luca, P. G. Medaglia, F. M. Granozio, et al., Phys. Rev. Lett. 102, 167401 (2009).

³⁴ L. Braicovich, J. van den Brink, V. Bisogni, M. M. Sala, L. J. P. Ament, N. B. Brookes, G. M. De Luca, M. Salluzzo,

- T. Schmitt, V. N. Strocov, et al., Phys. Rev. Lett. **104**, 077002 (2010).
- M. Guarise, B. D. Piazza, M. M. Sala, G. Ghiringhelli, L. Braicovich, H. Berger, J. N. Hancock, D. van der Marel, T. Schmitt, V. N. Strocov, et al., Phys. Rev. Lett. 105, 157006 (2010).
- ³⁶ L. J. P. Ament, G. Ghiringhelli, M. M. Sala, L. Braicovich, and J. van den Brink, Phys. Rev. Lett. 103, 117003 (2009).
- ³⁷ J. Luo, G. T. Trammell, and J. P. Hannon, Phys. Rev. Lett. **71**, 287 (1993).
- ³⁸ P. Carra and B. T. Thole, Rev. Mod. Phys. **66**, 1509 (1994).
- ³⁹ T. Tonegawa, Prog. Theor. Phys. **40**, 1195 (1968).
- ⁴⁰ C. C. Wan, A. B. Harris, and D. Kumar, Phys. Rev. B 48, 1036 (1993).

- ⁴¹ L. J. P. Ament, M. van Veenendaal, T. P. Devereaux, J. P. Hill, and J. van den Brink, Rev. Mod. Phys. 83, 706 (2011).
- J. P. Hannon, G. T. Trammell, M. Blume, and D. Gibbs,
 Phys. Rev. Lett. 61, 1245 (1988).
- ⁴³ M. W. Haverkort, Phys. Rev. Lett. **105**, 167404 (2010).
- ⁴⁴ J. Igarashi, J. Phys. Soc. Jpn. **62**, 4449 (1993).
- ⁴⁵ J. I. Igarashi and T. Nagao, Phys. Rev. B **72**, 014403 (2005).
- ⁴⁶ D. Vaknin, S. K. Sinha, D. E. Moncton, D. C. Johnston, J. M. Newsam, C. R. Safinya, and H. E. King Jr., Phys. Rev. Lett. **58**, 2802 (1987).
- ⁴⁷ G. Aeppli, S. M. Hayden, H. A. Mook, Z. Fisk, S. -W. Cheong, D. Rytz, J. P. Remeika, G. P. Espinosa, and A. S. Cooper, Phys. Rev. Lett. **62**, 2052 (1989).